

Paleoseismology and Geomorphology of the Raymond Fault, Los Angeles County, California

by Kristin D. Weaver* and James F. Dolan

Abstract The Raymond fault extends for 20 km in a broad convex-to-the-south arc across the densely populated San Gabriel Valley northeast of Los Angeles. Although south-facing scarps characterize much of the fault, geomorphic and seismological evidence indicate a predominance of left-lateral motion. An apparent 3.4-km left-lateral offset of a crystalline basement ridge at the east end of the fault may approximate total slip on the fault. Data from one of our paleoseismologic trenches, in combination with published data, indicate that the most recent Raymond fault surface rupture occurred $\sim 1\text{--}2$ ka. Estimates of fault-plane area suggest that rupture of the entire Raymond fault could generate an earthquake of $M_w \sim 6.7$. The similar kinematics of the Raymond fault and the Hollywood fault, along strike to the west, together with a pronounced fault-parallel gravity lineament and sparse geomorphic evidence, suggests that there may be a through-going mechanical connection between the two faults, and that they could conceivably rupture together in large earthquakes. Published data, however, indicate that the Hollywood fault ruptured to the surface most recently $\sim 6\text{--}9$ ka, indicating that the most recent Raymond fault surface rupture apparently did not extend westward onto the Hollywood fault. Data from another of our paleoseismologic trenches yielded evidence for at least five latest Pleistocene earthquakes, including at least four surface ruptures that occurred during a brief, $\leq 10,000$ -year-long period between ~ 31.5 and 41.5 ka. The ≤ 3300 year-long, average recurrence interval for these events is much shorter than the interval suggested for the past $\sim 40,000$ years by the frequency of paleoearthquakes recognized in previous trenches. Thus, either the 31.5 ka to 41.5 ka events represent a temporal cluster, and the recurrence interval for the fault is highly irregular, or at least half of all Raymond fault earthquakes that have occurred since ~ 31.5 ka have not yet been recognized.

Introduction

The city of Los Angeles is built atop a major transition between two tectonic provinces. To the south, northwest-trending right-lateral strike-slip faults accommodate most plate-boundary strain. In contrast, the northern part of the urban area is dominated by generally west-trending reverse faults and left-lateral strike-slip and oblique-slip faults (e.g., Ziony and Jones, 1989; Wright, 1991; Dolan *et al.*, 1995; Walls *et al.*, 1998; Fig. 1). Over the past several decades, the complicated network of faults beneath the northern half of the urban area has generated a number of moderate to moderately large earthquakes, including the 1971 M_w 6.7 San Fernando, the 1987 M_w 6.0 Whittier Narrows, the 1991 M_w 5.8 Sierra Madre, and the 1994 M_w 6.7 Northridge events

(Scientists of USGS/SCEC, 1994). Geodetic observations indicate that the faults that generated these earthquakes lie within a narrow, east-trending belt of rapid north–south shortening (Walls *et al.*, 1998; Argus *et al.*, 1999).

Despite a heightened awareness of the potential hazards for destructive earthquakes beneath metropolitan Los Angeles, the earthquake histories, kinematics, locations, and geometries of many of these faults remain poorly known. In this article we describe results of a paleoseismic and geomorphic analysis of the Raymond fault, an east-northeast-trending, left-lateral strike-slip fault located just northeast of downtown Los Angeles, within the zone of geodetically determined, rapid north–south shortening. We discuss the implications of our results for seismic hazard assessment in the region and compare our paleoseismologic observations with similar observations from adjacent faults.

*Present Address: William Lettis and Associates, 25050 Avenue Kearney, Suite 108, Valencia, California 91355.

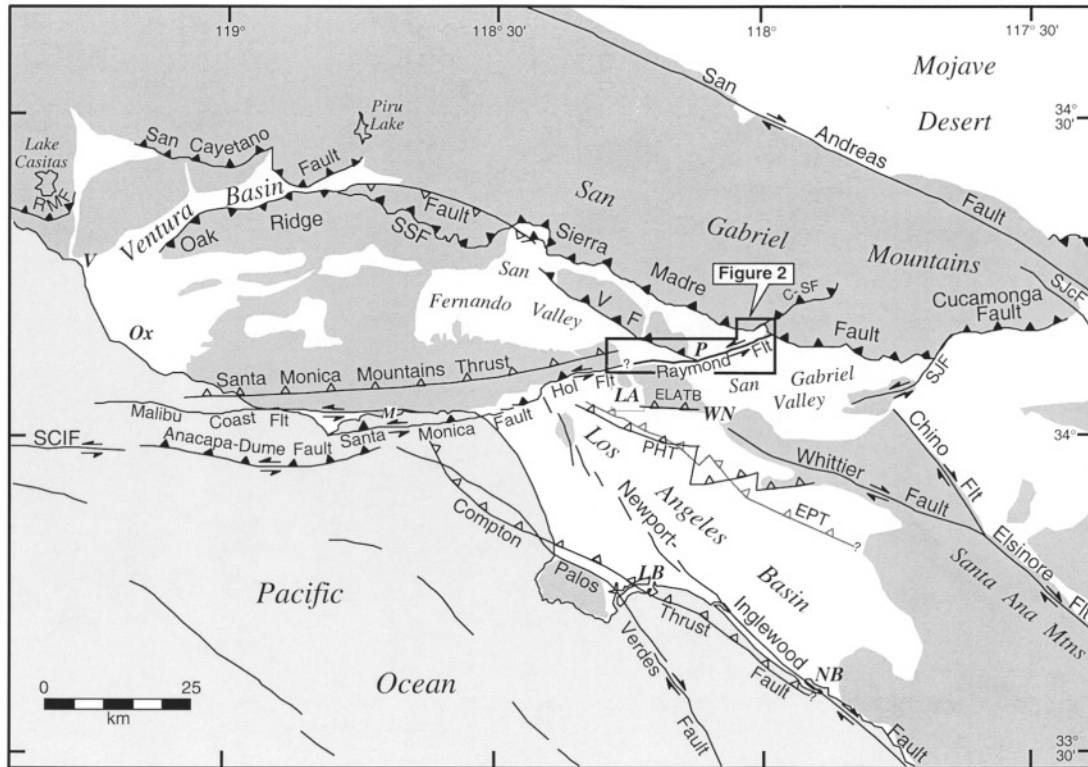


Figure 1. Regional neotectonic map for metropolitan southern California showing major active faults (slightly modified from Dolan *et al.*, 1997). Fault locations are from Ziony and Jones (1989), Vedder *et al.* (1986), Dolan and Sieh (1992), Shaw and Suppe (1995), and Shaw and Shearer (1999). Closed teeth denote reverse-fault surface traces; open teeth show upper edges of blind thrust fault ramps. Strike-slip fault surface traces identified by double arrows. C-SF, Clamshell-Sawpit fault; ELATB, East Los Angeles thrust belt; EPT, Elysian Park blind thrust fault; Hol Ftl, Hollywood fault; PHT, Puente Hills blind thrust fault; RMF, Red Mountain fault; SCIF, Santa Cruz Island fault; SJcF, San Jose fault; SSF, Santa Susana fault; VF, Verdugo fault; LA, Los Angeles; LB, Long Beach; M, Malibu; NB, Newport Beach; Ox, Oxnard; P, Pasadena; SJcF, San Jacinto fault; V, Ventura; WN, Whittier Narrows. Dark shading shows Santa Monica Mountains.

Geomorphology

The 20-km-long Raymond fault trace is gently arcuate, convex-to-the-south, and extends across the San Gabriel Valley south of the San Gabriel Mountains (Fig. 1). The fault is well-defined geomorphically as a predominately left-lateral strike-slip fault with minor north-side-up motion, as shown by common left-lateral stream offsets and south-facing scarps ranging in height from <1 m to as much as 45 m (Fig. 2; Buwalda, 1940; Crook *et al.*, 1987). The geomorphology is consistent with the nearly pure left-lateral focal mechanism determined for the M_L 4.9 1988 Pasadena earthquake, which nucleated at a depth of 16 km (Jones *et al.*, 1990). When plotted with its aftershocks, the focal plane of the 1988 earthquake lies on a 80°-north-dipping plane that projects up to the surface trace of the Raymond fault (Jones *et al.*, 1990; Fig. 3).

Pronounced lateral changes in geomorphic character and fault orientation allow us to define five distinct zones along the length of the fault, designated as Zones I through

V, from east to west (Figure 2). The eastern end of Zone I marks the Raymond fault's intersection with the Sierra Madre fault, a 90-km-long, north-dipping reverse fault that extends along the southern edge of the San Gabriel Mountains (Crook *et al.*, 1987; Ziony and Jones, 1989; Wright, 1991; Dolan *et al.*, 1995; Walls *et al.*, 1998). Zone I is 3.4 km long and is characterized by south-facing scarps along the southern edge of a 150-m-high, crystalline basement ridge. Along this reach the Raymond fault separates the crystalline rocks to the north from Quaternary alluvium to the south. Zone I extends westward to Santa Anita Wash, a major south-flowing drainage emanating from the San Gabriel Mountains.

Zone II, which stretches for 2.4 km westward from Santa Anita Wash (Fig. 2), is characterized by nearly continuous, southwest- and southeast-facing scarps. These scarps are associated with two left (releasing) bends, where scarps face southeast, and two pressure ridges (8 and 9 in Figure 2) formed along right (restraining) bends in the fault (Buwalda, 1940).

Zone III begins just west of pressure ridge 8 (Fig. 2).

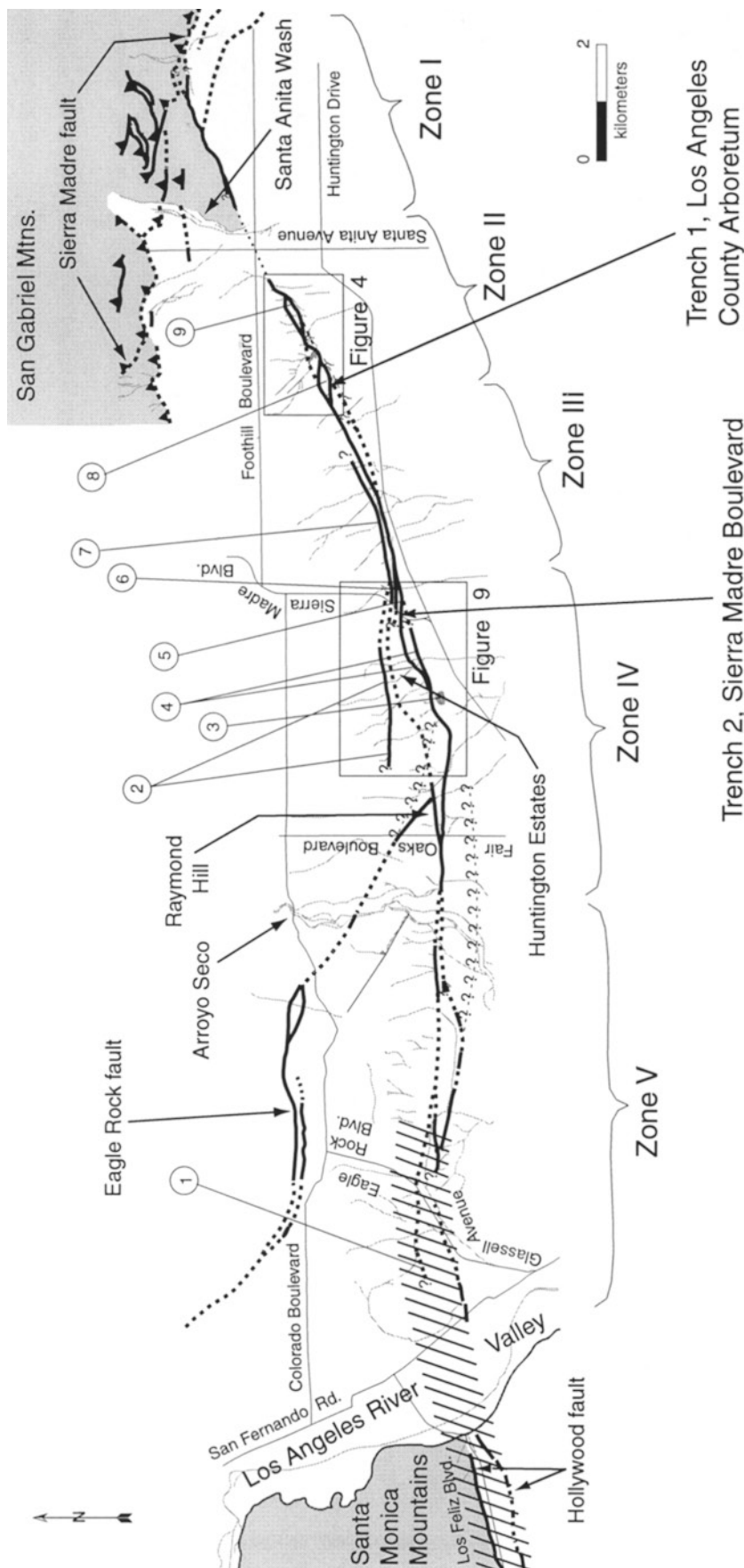


Figure 2. Strip map showing strands of the Raymond fault, fault-related features, geomorphic zones, and study sites discussed in the text. Heavy black lines are faults. Thin, pale gray lines and thin black lines represent drainage patterns and selected streets, respectively. Hatchured area shows the gravity lineament that may represent a through-going fault connection between the Raymond and Hollywood faults (Hill *et al.*, 1979; Chapman and Chase, 1979). Fault locations have been modified from Weber *et al.* (1980), Crook *et al.* (1987), Dibblee (1989a and b) and Dolan *et al.* (1997). Numbered sites are as follows: (1) inferred north-side-down fault (Weber *et al.*, 1980); (2) drainages offset left-laterally 180 to 300 m; (3) Lacy Park sag pond; (4) two scarps at Huntington Estates; (5) pressure ridge; (6) spring in Rubio Wash/Crook *et al.* (1987) trench; (7) spring in gully/Crook *et al.* (1987) trench; (8) pressure ridge; (9) pressure ridge. Boxes show the locations of detailed topographic maps of the two study sites discussed in the text.

$M_L = 4.9$ 1988 Pasadena Earthquake

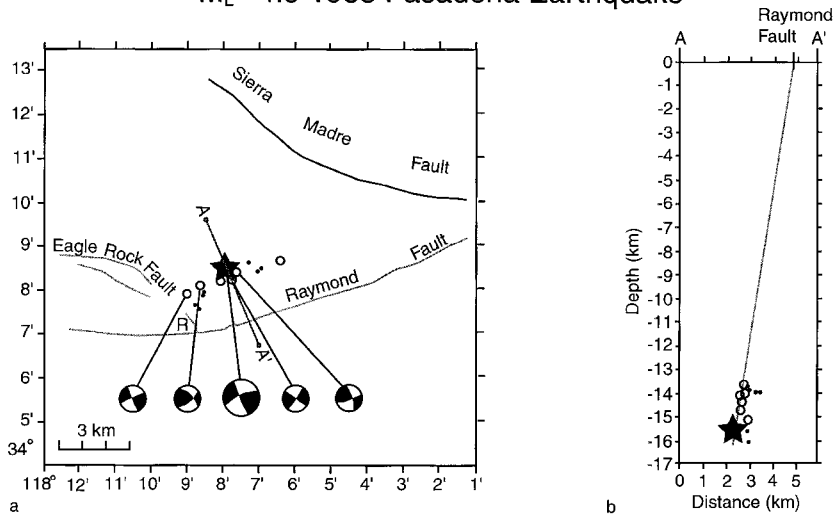


Figure 3. (a) Map showing the locations of the 3 December 1988 $M_L = 4.9$ Pasadena earthquake (solid star) and its aftershocks together with focal mechanisms for the mainshock and the four largest aftershocks (compressional quadrants shown in black) (from Jones *et al.*, 1990). R is Raymond Hill. (b) Cross section showing the hypocenters of the Pasadena earthquake and its aftershocks projected onto the plane A-A', shown in 4a (From Jones *et al.*, 1990). Note that the mainshock and aftershocks lie on a plane that projects to the surface trace of the Raymond fault.

Although this zone includes low (≤ 5 m), south-southeast-facing scarps, they are much less pronounced than to the east and west along zones II and IV. Zone III is 3.5 km long and consists of at least three fault strands, all of which exhibit predominately strike-slip fault geomorphic features, including several streams that have been deflected to the left by 30 to 300 m, beheaded streams, shutter ridges, closed depressions, and ground water and vegetation lineaments (Buwalda, 1940; Crook *et al.*, 1987; Jones *et al.*, 1990). In addition, many back-tilted, gently north-dipping alluvial surfaces occur along the northern margin of the fault zone along this reach. Zone III extends westward to the eastern end of a pressure ridge at the eastern end of zone IV (5 in Figure 2).

Highly dissected hills with south-facing scarps characterize the 5.5-km-long zone IV. These hills (4 in Figure 2), increase in elevation westward towards a 25° restraining bend. The top of the scarps are as much as 45 m above the alluvial fans to the south, and they are deeply incised by several large drainages. A sag pond (now occupied by Lacy Park) occurs at a small left step within this large right bend (3 in Figure 2). At least one fault strand in zone IV exhibits several stream channels that have been deflected to the left by 180 to 300 m (2 in Figure 2).

Zone V stretches for 7.6 km from Arroyo Seco to the Los Angeles River. On the western side of Arroyo Seco the Raymond fault is characterized by two major, subparallel strands that bound a linear, west-trending depression (Fig. 2) (Buwalda, 1940; Crook *et al.*, 1987). Farther to the west, Dibblee (1989) noted a north-facing scarp that may be the connection between the Raymond fault and the Hollywood fault west of the Los Angeles River (1 in Figure 2).

The Raymond fault and the Hollywood fault, along strike to the west, have similar trends, and both show evidence for oblique-reverse, left-lateral displacement (Dolan *et al.*, 1995, 1997, 2000a; Fig. 2). Despite these similarities,

it is difficult to confidently connect these two faults on the basis of geomorphic expression alone, because the area between the faults lies largely along the floodplain of the Los Angeles River. However, several east-trending linear features, including potential scarps and a pronounced gravity lineament, extend between Arroyo Seco and the Hollywood fault along the approximate strike of the Raymond fault, suggesting that a through-going mechanical connection may exist between the Raymond and Hollywood faults (Figure 2; Chapman and Chase, 1979; Weber *et al.*, 1980; Crook *et al.*, 1987; Dibblee, 1989, 1991; Dolan *et al.*, 1997). Several workers have also attempted to establish mechanical continuity between the Raymond fault and the Eagle Rock fault (Weber *et al.*, 1980; Crook *et al.*, 1987). The exact location of the Eagle Rock fault, however, is poorly known, because it is not well-defined geomorphically, and such a connection cannot be confidently established on the basis of geomorphologic observations.

Paleoseismic Observations Along the Raymond Fault

Previous Work

As part of a seismic hazard analysis of the northern Los Angeles metropolitan region, Crook *et al.* (1987) excavated a number of paleoseismologic trenches, including several across the Raymond fault (e.g., 6 and 7 in Figure 2). They reported evidence for at least five, and possibly as many as eight, Raymond fault surface ruptures since 36,000 radiocarbon years B.P., suggesting a minimum recurrence interval of 5,000 to 9,000 years. The rate of production of ^{14}C , however, has not been constant through time, and the true "calendaric" age of the 36,000 B.P. sample is older than its age in radiocarbon years by several thousand years (e.g., Voelker *et al.*, 1998). This sample is older than the oldest samples that can be calibrated with Calib 3.0.3 (Stuiver and Reimer,

1993), but we can estimate its approximate calendric age by applying a correction to the radiocarbon age based on coral and lake sediment age data in conjunction with a geomagnetic models of magnetic flux intensity and comparisons of high-resolution sediment records with precisely dated ice cores (Bard *et al.*, 1993; 1998; Laj *et al.*, 1996; Voelker *et al.*, 1998). These studies indicate that the approximate calendric age for the ~36,000 year B.P. sample is ~40.5 to 41 ka (Voelker *et al.*, 1998). This age would suggest a measured minimum recurrence interval for the Raymond fault based on the Crook *et al.* (1987) paleoseismologic data of ~5,700 to ~10,250 years. Crook *et al.* (1987), however, recognized that additional events may have remained undetected in their study, and speculated that the actual average recurrence interval was shorter. They suggested 3,000 years as a plausible recurrence interval for the Raymond fault surface ruptures.

This Study

We used published geologic maps (Buwalda, 1940; Crook *et al.*, 1987; Dibblee, 1989, 1991), 1:24,000 scale topographic maps, vintage aerial photographs collected between 1928 and the 1980s, and field reconnaissance to identify the main traces of the Raymond fault. We excavated paleoseismologic trenches at two sites along the most recently active trace of the fault (Fig. 2).

Los Angeles County Arboretum Site. We excavated our first trench (T-1) at the Los Angeles County Arboretum, near the east end of geomorphic zone III (Figs. 2 and 4). Previous trench excavations by Crook *et al.* (1987) on the north side

of a 500-m-long, 22-m-high, west-trending pressure ridge yielded no paleoseismic information, but did expose possible evidence for a south-dipping splay of the fault that deformed Pleistocene and Holocene alluvium. We excavated a 42-m-long trench (T-1) across the southern scarp of the pressure ridge (Figs. 4 and 5). The north end of the trench was located ~2 m south of the access road that winds around the pressure ridge, and the trench terminated about 1 m north of the Arboretum property boundary (Fig. 5).

Stratigraphy. Trench T-1 exposed well-bedded, predominantly sandy and silty strata that can be divided into three structural blocks, separated by two strands of the fault (Fig. 5). The northernmost structural block (north of fault a) consists of weakly consolidated sands overlain by a silty sand bed, with 2 m of sandy gravels above. The gravels grade upwards over ~40 cm into poorly sorted gravels (unit B). Based on the orange-brown color of unit B and the abundance of illuvial clay in the sandy gravel, we interpret this unit as an argillic (B_t) soil horizon. The B_t horizon is capped by 40–60 cm of dark brown, organic-rich, silty sand (unit A), which pinches out to the south at the surface projection of fault a. We interpret this uppermost unit as the A horizon of the surface soil.

The middle block is bounded by fault a to the north and fault c to the south (Fig. 5). The stratigraphy in the lower three meters of the middle block is similar to that of the northern block, with a basal section consisting of gently south-dipping, interfingering sands and silts, overlain by gently south-dipping gravels. These gravels are overlain by two bioturbated, wedge-shaped silty sand units. The lower wedge-shaped de-

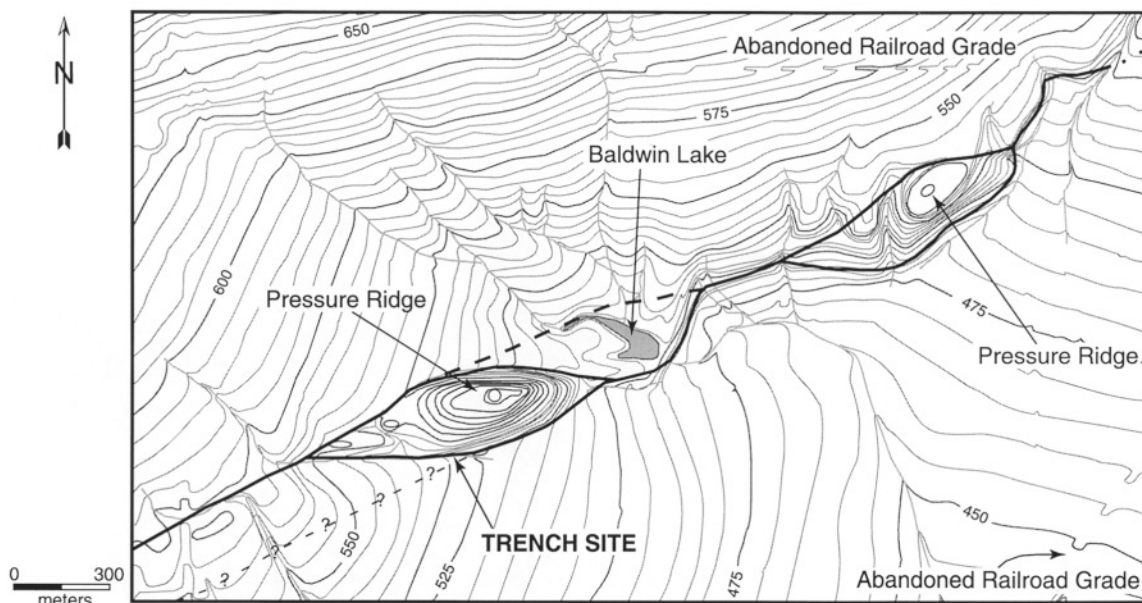


Figure 4. Detail of the 1928 USGS 6' Sierra Madre Quadrangle topographic map showing the site of T-1 trench and the geomorphic expression of the Raymond fault in this area. Bold lines indicate splays of the Raymond fault and light lines indicate drainages. Elevations are in feet above mean sea level. Based on Crook *et al.* (1987) and our own geomorphologic mapping. Contour interval is 5 feet.

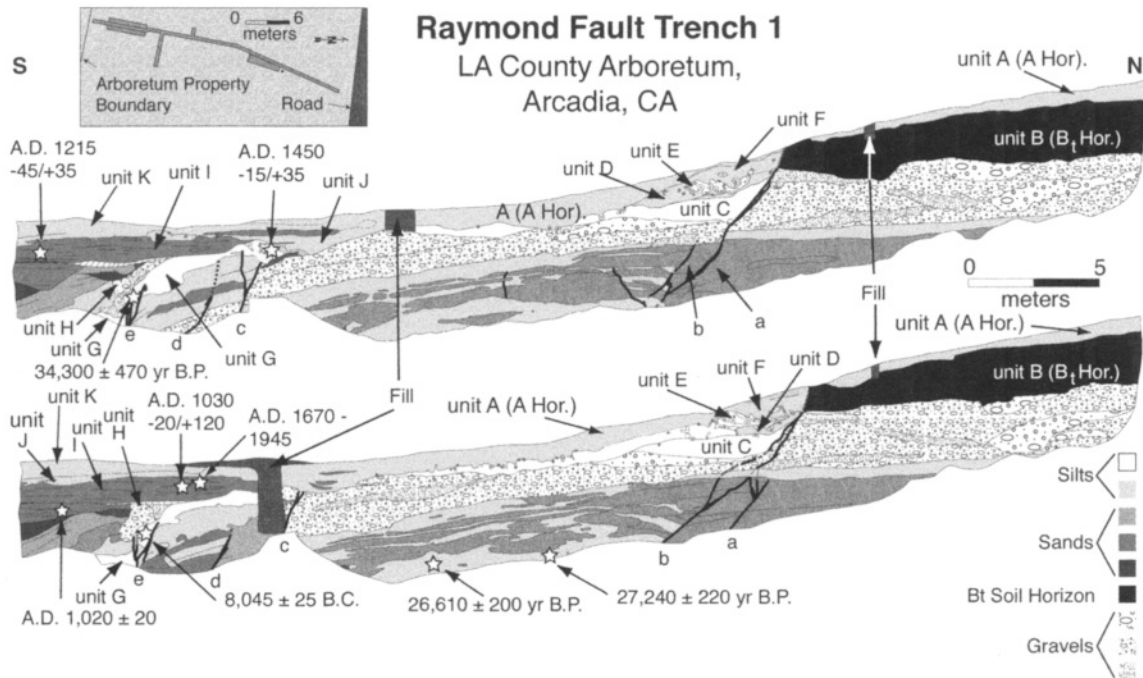


Figure 5. Logs of the west and east walls of trench T-1. Faults are shown by heavy black lines. Stars show locations of detrital charcoal samples. Note that the east wall (bottom diagram) is shown as a mirror image to facilitate comparison with the west wall. Inset map at the top shows the layout of this trench site.

posit consists of massive silt (unit C), while the overlying unit is made up of several deposits that can be further subdivided into several smaller-scale, distinct wedge-shaped deposits (units D through F). These units are capped by a 1-m-thick, dark brown, organic-rich A horizon that pinches out to the north at the surface projection of fault a (Fig. 6).

The southern structural block consists of cobble to pebble gravels overlain by interfingering sand and silt layers that include unit G (Figs. 5 and 7). These deposits dip moderately to steeply to the south and are covered by several pebble to cobble gravel channels. One of the younger channels (unit H) appears to have preferentially eroded into fault zone e (Fig. 7). Several of these channels grade upward into a sequence of moderately south-dipping, well-stratified sands and pebble gravels, which are in turn overlain by a package of horizontal, finely bedded, medium- to coarse-grained sand and granules beds (unit I). The unit I sand and granule beds overlie the upward terminations of faults c and d. A gray, well-stratified, silty sand (unit J) covers the friable sands and gravels. Unit J is itself overlain by a darker gray, stratified, organic-rich silty sand (unit K).

Over most of the length of the trench south of fault a, the shallowest units do not appear to be typical A horizons. Typical of most well-developed A horizons, the active A horizon (unit A) is generally thoroughly bioturbated, with no original bedding discernible. In contrast, the near-surface, dark-gray-brown deposits south of fault strand a (units J and K) contain many unbioturbated to weakly bioturbated, thin

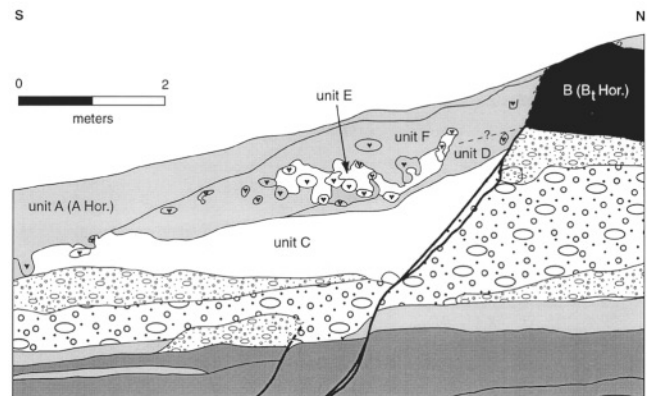


Figure 6. Detail of log of west wall of trench T-1 illustrating relationship between upper part of fault a-b and wedge-shaped units C-F. Patterns are the same as in Figure 5.

beds and lenses of pale yellow-brown sand, as well as beds of alternating darker gray and paler gray silty sand. This well-preserved stratification indicates that the A horizon material to the south of fault a has been reworked. We interpret these units as youthful deposits of A horizon material that have been washed down the slope and deposited nearer the base of the pressure ridge.

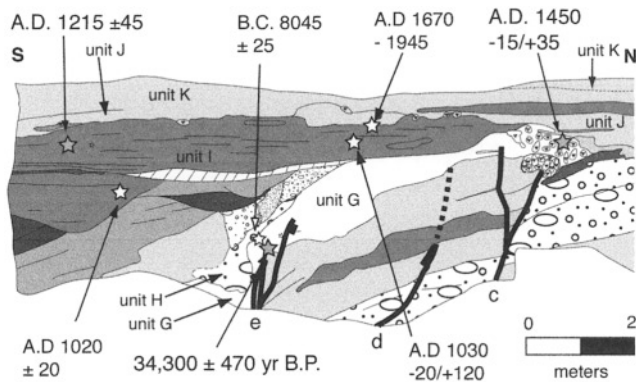


Figure 7. Diagram of the south end of the west wall of trench T-1 showing the relationship of undeformed units to deformed units. Faults c, d, e, and f are indicated by bold lines. Hatchured region indicates slough on the benched portion of the trench. White and gray stars show locations of detrital charcoal samples collected for age analyses from the east and west trench walls, respectively. Patterns are same as in Figure 5.

Age Control. We collected 10 pieces of detrital charcoal for radiocarbon analysis from Trench 1 (Table 1). Three samples, two of which were combined to provide sufficient carbon for a successful accelerator mass spectrometer (AMS) age analysis, were collected from the fine-grained silty sands at the base of the trench from the middle structural block (Fig. 5). These two AMS analyses yielded radiocarbon ages of $27,240 \pm 220$ yr B.P. and $26,610 \pm 200$ yr B.P. These ages in radiocarbon years are equivalent to corrected, approximate calendric ages of ~ 31 ka, based on Voelker *et al.* (1998).

The remaining seven charcoal samples came from the southern stratigraphic block (Fig. 7). One of these yielded an AMS date of $34,000 \pm 470$ radiocarbon years B.P.; this sample, however, was collected from unit G, which also yielded a calibrated, calendric date of B.C. 8045 ± 25 yr, indicating that the 34 ka sample is reworked (all samples reported as calendric ages were calibrated using Calib 3.0.3; Stuiver and Reimer, 1993). One sample collected from the lower part of unit I yielded a calendric date of A.D. 1020 ± 20 yr. Three other pieces of detrital charcoal from unit I yielded calibrated, calendric dates of A.D. $1030 -20/+120$ yr, A.D. 1215 ± 45 yr, and A.D. 1670–1945, in stratigraphic succession. The shallowest sample, which is substantially younger than the others, was collected from only 2 cm below a lens of gray, silty, fine- to medium-grained sand that we interpret as reworked A horizon material. Based on the date and the proximity of the sample to the reworked A horizon material, we suspect that it was introduced into unit I by bioturbation, probably along an unrecognized burrow. The tenth sample, which was collected from the silty sand (unit G in Figures 5 and 7) just below the A horizon, yielded a

calibrated, calendric age of A.D. $1450 + 35/-15$. This sample was collected from a highly bioturbated, predominately massive section. Based on its proximity to numerous animal burrows mapped at the base of the A horizon, and the young radiocarbon age it yielded, we believe this sample was also collected from an unrecognized animal burrow, and that its age is therefore not meaningful.

Evidence for Faulting. The trench revealed two major fault zones comprising five fault splays. The northern fault zone (strands a and b on Figures 5 and 6) is a narrow, well-defined zone of faults at the base of the trench. Faults within this zone anastomose and separate upward into four and five planes on the east and west walls, respectively. Several of these fault planes terminate at a horizon ~ 3 m below the ground surface, but one fault continues upward and juxtaposes the argillic (B₁) horizon (unit B) against wedge-shaped unit E to the south (Fig. 6). This splay appears to reach the ground surface. The dark gray-brown, organic-rich active A horizon (unit A) pinches out where the fault projects to the surface. Strata to the north of faults a and b are horizontal, whereas strata to the south generally dip gently southward.

The 7-m-wide southern fault zone consists of three major strands that extend upward through the south-dipping strata exposed near the south end of the trench (Fig. 7). The northern and middle strands of the southern fault zone (strands c and d, respectively, in Figure 7) dip steeply to the south, whereas the southernmost strand (strand e) is near-vertical. Strand c juxtaposes cobble gravels in a sand matrix to the north with interfingering sands and silts to the south. The southernmost fault (strand e) comprises several closely spaced, vertical, anastomosing faults that are truncated upward by a set of narrow, trough-shaped channel deposits, which appear to have eroded down through the fault zone.

Interpretation of Trench 1 Results. In addition to the two major fault zones described already stratigraphic and structural relationships observed in the trench lead us to infer a fault zone to the south of our trench, beyond the Arboretum property boundary and inaccessible to trench excavations. This inferred fault zone is required to explain southward-tilting of the sand and granule layers at the south end of the trench. Although we did not expose all of the strands along the southern boundary of the Arboretum pressure ridge, we can use the structural and stratigraphic relationships exposed in the trench to provide constraints on the earthquake history of the Raymond fault at this site.

Central Fault Zone. Although south-dipping faults a and b in the central part of the trench exhibit apparent south-side-down normal separations in the upper 2 m, the lack of vertical separation of distinctive stratigraphic units below 2 m depth is mostly likely the result of nearly pure strike-slip offset that has juxtaposed laterally dissimilar stratigraphic sequences. In the upper 2 m, the fault separates cobble gravels capped by a 1.5-m-thick argillic horizon to the north of

Table 1
C¹⁴ Samples from Raymond Fault Trench 1, L.A. County Arboretum, Arcadia, CA

Sample*	Location†	Description	Conventional ¹⁴ C Age‡	Calibrated Calendar Year§	Approximate Calendric Ages based on Voelker <i>et al.</i> (1998)
RF 1 East wall	m 21.00, -3.84	Organic sediment; from silty fg ss layer at bottom of trench; same as RF 5 and 8	27,240 ± 220 B.P.	—	~31 ka
RF 3 West wall	m 32.60, -1.40	Detrital charcoal; from 20 cm below A horizon	430 ± 50 B.P.	A.D. 1450 - 15/+35	—
RF 5 East wall	m 21.77, -4.20	Organic sediment; from silty fg ss layer at bottom of trench; same as RF 1	26,610 ± 200 B.P.	—	~31 ka
RF 8 West wall	m 22.52, -3.71	Organic sediment; from silty fg ss layer at bottom of trench; same as RF 1 and 5 (RF 5 and 8 were combined)	—	—	—
RF 100 East wall	m 37.60, -3.10	Detrital charcoal; from fg ss in s. fault zone same as RF 102	9,030 ± 50 B.P.	A.D. 8,045 ± 25	—
RF 101 East wall	m 40.37, -1.51	Detrital charcoal; from horizontal cg ss at end of extension	1,000 ± 50 B.P.	A.D. 1020 ± 20	—
RF 102 west wall	m 37.43, -2.76	Detrital charcoal; from micaceous fg ss in s. fault zone; same as RF 100	34,300 ± 470 B.P.	—	~39 ka
RF 103 west wall	m 40.76, -1.20	Detrital charcoal; from cg ss at end of extension	850 ± 50 B.P.	A.D. 1215 - 45/+35	—
RF 106 east wall	m 35.85, -0.85	Detrital charcoal; from horizontal cg ss at end of extension	130 ± 70 B.P.	A.D. 1670-1945	—
RF 109 east wall	m 35.50, -1.00	Detrital charcoal; from horizontal cg ss at end of extension	980 ± 50 B.P.	A.D. 1030 - 20/+120	—
C-6 [#] Trench 7, Sunny Slope Reservoir	west wall	Bulk soil collected from within a fracture thought to be the result of the most recent surface rupture	2160 ± 105 B.P.	B.C. 189 - 117/+212	—

*All samples were processed by Beta Analytic, Miami, Florida, except that noted by #. All samples were pretreated with acid, alkali, and acid washes before analysis, except for those noted by ||.

†Please see Figure 5 and 9 for sample locations on the trench logs.

‡Conventional dates are reported as radiocarbon years before present (RCYBP), where "present" = 1950 A.D. and include two sigma, or 95% probability, error bars.

§Calibrated Calendar Years were calculated by the lab using the Pretoria Calibration Procedure program, and include one sigma error bar. Some sample Conventional ages were too old to fit to the calibration curves and are designated by dashes.

||Indicates sample that the sample was acid-washed only.

#Indicates a sample collected and dated by Crook and others (1987).

the fault zone from the massive, wedge-shaped deposits to the south (Fig. 6).

The two wedge-shaped deposits to the south of faults a and b (comprising units C, and D-E-F) were exposed in three faces: the two original trench walls, and a later exposure excavated 3 m to the east of the original east wall of the trench (Fig. 8). The origin of these wedge-shaped deposits remains unclear. If the stratigraphic relationships exposed lower in the trench did not preclude major south-side-down normal displacements along this strand of the fault, we would interpret these as colluvial wedges shed from a south-dipping oblique-normal fault scarp. But since the strata exposed below the wedges do not exhibit any vertical separations across the fault, the wedges must be either: (1) colluvial

wedges shed off a south-facing scarp caused by strike-slip or oblique-strike-slip juxtaposition of irregular topography; or (2) channel deposits. Geometrically, the wedges appear to extend along the strike of the fault, which is, of course, along the scarp. This relationship suggests that if these are channel deposits, then the channel must have been flowing along the fault. We believe, however, that the coincidence of the north edge of the deposit with the upward projection of faults a and b argues against this being a purely sedimentary contact, and that the contact is a fault that extends all the way to the ground surface. This inference is supported by the fact that the wedge-shaped deposits are massive and are composed of what appears to be, at least in part, old A horizon material, suggesting that they may be colluvial

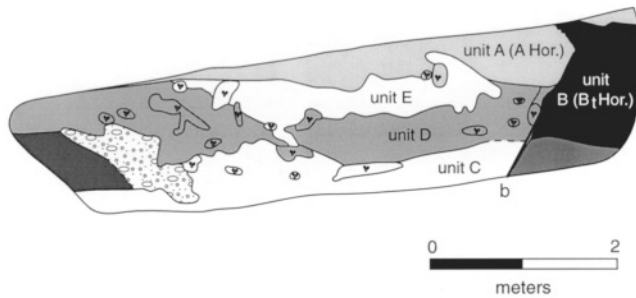


Figure 8. Log of east wall (mirror image) of trench face excavated 3 m to the east of the original eastern wall of trench T-1 showing details of the upward termination of the south-dipping, central fault zone observed in trench T-1. Patterns are the same as in Figure 5.

wedges related to lateral offset of irregular topography. In contrast, all of the channel deposits that we observed elsewhere in the trench were pervasively and finely bedded on the millimeter to centimeter scale. If units C and D-E-F are colluvial wedges, then they record at least two distinct surface ruptures of the central strand of the Raymond fault at this site. The three detrital charcoal ages recovered from the base of the central block provide a maximum age for the wedge-shaped deposits described earlier, suggesting two earthquakes have occurred on these fault strands since $\sim 27,000$ radiocarbon years B.P. (equivalent to a corrected, approximate calendric age of ~ 31 ka; Voelker *et al.*, 1998).

Southern Fault Zone. The 5-m-wide southern fault zone, comprising faults c, d, and e, cuts upward through south-dipping strata, including unit G, but does not cut overlying horizontal unit I (Figs. 5 and 7). On the west wall, fault d cuts several strata without any apparent vertical separation, whereas stratigraphic relations across fault c suggest a component of apparent south-side-down separation. In contrast, on the east wall (Fig. 5), strand d juxtaposes differing stratigraphic units, whereas strand c juxtaposes gravels that appear to be the same unit. These relations suggest that the faulted units are laterally discontinuous and that fault splays c and d have experienced predominately horizontal motion.

The southernmost fault strand, fault e, may also accommodate some of the horizontal motion along the Raymond fault, but the relationship between fault e and adjacent strata suggest a component of north-side-up motion, as well. Note that unit G (Fig. 7) is gently south-dipping at its northern end, but becomes steeper at fault e. The upper contact of this unit appears to have been modified during erosion by the overlying channel (unit H in Figure 7), but the lower contact of unit G has been juxtaposed with the underlying units in a north-side-up relationship.

The B.C. 8050 AMS date obtained from deformed and faulted unit G provides a maximum possible age for the most recent surface rupture along the southern strand. As discussed already, these faulted, tilted strata are overlapped by

the horizontal, well-bedded sand, granule, and pebble beds of unit I, from which we obtained three stratigraphically consistent calendric ages, A.D. 1020 ± 20 , A.D. $1030 - 20/+120$, and A.D. 1215 ± 45 , which do not appear to have been contaminated by recent A horizon material. These age data indicate that the most recent tilting event on the southern fault strand exposed in Trench T-1 occurred at least 1000 years ago, and sometime after \sim B.C. 8050.

Sierra Madre Boulevard Site. Our second paleoseismologic trench (T-2) was excavated along the median strip of Sierra Madre Boulevard in the City of San Marino, California, ~ 4 km west-southwest of trench T-1 (Fig. 2). Aerial photograph analysis and geomorphic mapping of the site show that Sierra Madre Boulevard follows a man-modified stream channel through the eastern end of a west-trending line of hills. Earlier research (Crook *et al.*, 1987), coupled with our aerial photograph analysis, suggested that the fault zone at this location exhibits multiple anastomosing strands, and may be as wide as 400 m (Fig. 9). In order to better define the main active fault trace(s) at this site prior to excavating a trench, we excavated nine, 70-cm-diameter boreholes (commonly known as “bucket-auger” holes) along a 240-m-long, northeast-trending transect (Fig. 10).

Correlation of strata in boreholes 1, 2, 3, 5, and 9 revealed a very gently south-dipping, apparently undeformed alluvial sequence of silty sands and gravels (Figs. 10 and 11). In contrast, boreholes 4, 6, and 7 penetrated much more friable pebble gravels and fine- to coarse-grained sands that were distinctly different from the strata encountered in the more southerly boreholes. We drilled boreholes 7 and 8 between the two groups of boreholes, where we suspected a structural discontinuity existed.

Discrete faults were directly observed in two of the nine boreholes. Borehole 3 penetrated several small-scale, steeply south-dipping faults at 1 to 4 m depth. These faults disrupt many layers of finely laminated, iron-oxide-stained sands and silty sands and show only ~ 1 to 10 cm of vertical separation. Borehole 8 penetrated a larger-displacement fault, which dips steeply to the north and juxtaposes near-black to dark blue-gray, organic-rich, silty fine-grained sands on the north with iron-oxide-stained, medium- to fine-grained sands and silty sands to the south. In borehole 8 this fault could only be traced from 4 m depth to about 30 cm depth. The fault is truncated above by a dark gray, organic rich, silty sand through which the A horizon of the active surface soil has developed. We observed a second, approximately vertical fault in borehole 8 at ~ 8 m depth.

We also conducted a ground-penetrating RADAR (GPR) survey of the fault zone in order to locate any structures that may have been missed by the borehole transect (Fig. 12). We acquired a series of overlapping GPR profiles that spanned the entire suspected 400 m width of the fault zone at the Sierra Madre Boulevard site. The only major potential fault that was imaged by the GPR was a vertical discontinuity from very reflective strata to the north and

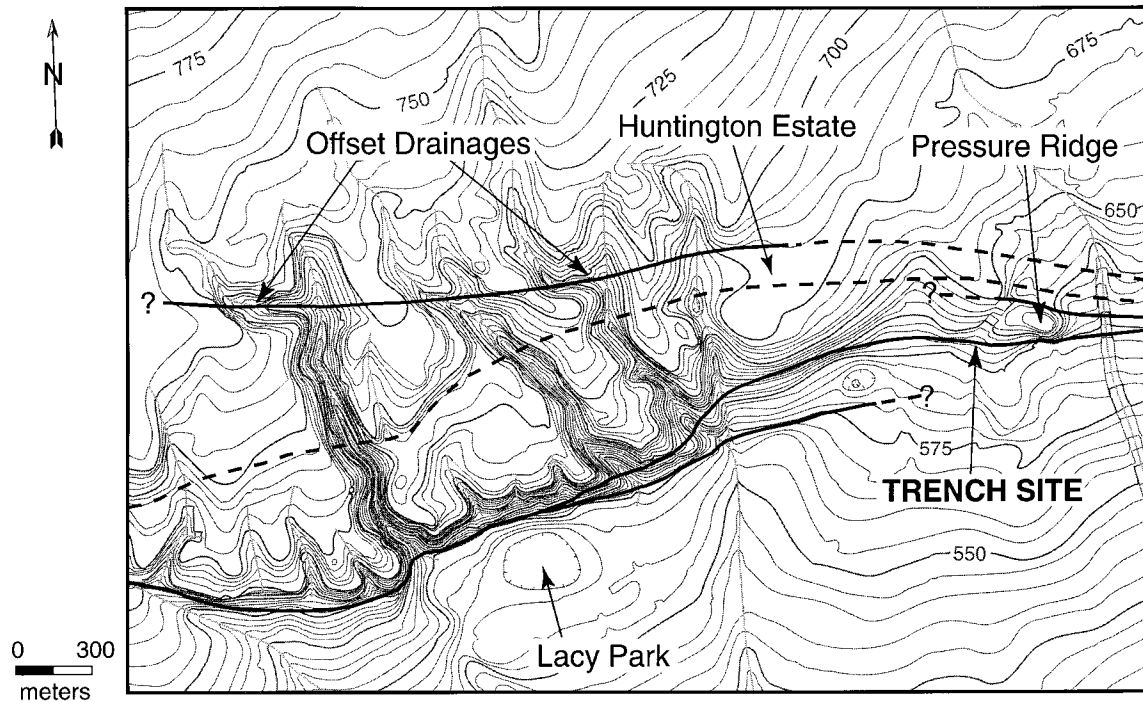


Figure 9. Detail of the 1928 USGS 6' Altadena Quadrangle topographic map showing the site of trench T-2 and the geomorphic expression of the Raymond fault in this region. Bold lines indicate splays of the Raymond fault and light lines indicate drainages. Elevations are in feet above mean sea level. Contour interval is 5 feet.

nonreflective strata to the south corresponding to the contact between the friable and cohesive strata between boreholes 7 and 8. The borehole and GPR data thus suggest that this structure, which is described in detail later, is the major active strand of the Raymond fault at this site.

Stratigraphy. In order to directly observe the entire fault zone identified in the bucket-auger borehole and GPR transects, we excavated a 28-m-long, 5-m-deep trench (T-2) that extended from 4 m south of borehole 3 to 2 m north of borehole 7. The trench revealed two main fault zones, each comprising several smaller faults (strands a–d in Figure 13) that cut through predominately flat-lying, to gently south-dipping alluvium (Fig. 13). The trench exposed two distinct stratigraphic sections that are separated by a nearly vertical fault (fault b), near the north end of the trench (Fig. 13). The package to the north of the fault consists of predominately friable sands and gravels that are locally cut by two other, near-vertical faults (a_1 and a_2); these strata will be discussed later. Many strata to the south of fault b can be traced near-continuously to the south end of the trench. The strata exposed between faults b and d generally dip gently (15° to 25°) to the south and consist of cohesive silty sand, sand, and pebble gravel beds. North-dipping strand d displaces this stratigraphic section, but units can be correlated across the fault. Strata to the south of fault d are generally flat-lying.

The base of the stratigraphic block bounded by faults b and d consists of ~ 10 layers of sand and silty sand (below

unit A in Figure 14) that vary from 10 to 30 cm in thickness. These are overlain by ~ 1 m of crudely stratified pebbly, sandy gravel (unit A), which is cut by several strands of fault c. The gravel is overlain by 40 cm of sandy silt (unit B), which is not cut by fault c. Unit B is in turn covered by an unstratified, reddish-brown sandy silt (unit C), which grades both upward and laterally into a 1.5-m-thick section of dark blue-gray to black, sandy clayey silt (unit D). Units C and D appear to be texturally similar, and differ only in color. Based on its very fine grain size and high organic content, we interpret unit D as an oxygen-starved marsh deposit. The close spatial association between the reddish-brown silt of unit C adjacent to faults b and d leads us to interpret the reddish-brown color of unit C to be a result of the presence of oxidizing fluids flowing along the faults.

At the top of the dark bluish-gray to black silt unit is a thin (≤ 10 cm) layer of charcoal-rich, black clayey silt, which is overlain by a sequence of sandy silts beds (units E, G, I, K, and M in Figure 14) and interfingering sand units (units H, J, L, and N). These beds generally dip gently (10° to 25°) southward, except at their northernmost extent, where they locally dip as steeply as 45° southward. Silt stringers occur within the sand units, and the internal stratigraphy is disrupted in several locations. A pebble and cobble gravel channel on the west wall (unit F) separates the lowest silt unit into two parts (units E and G in Figure 14).

The sands and silts within the fault-bounded block be-

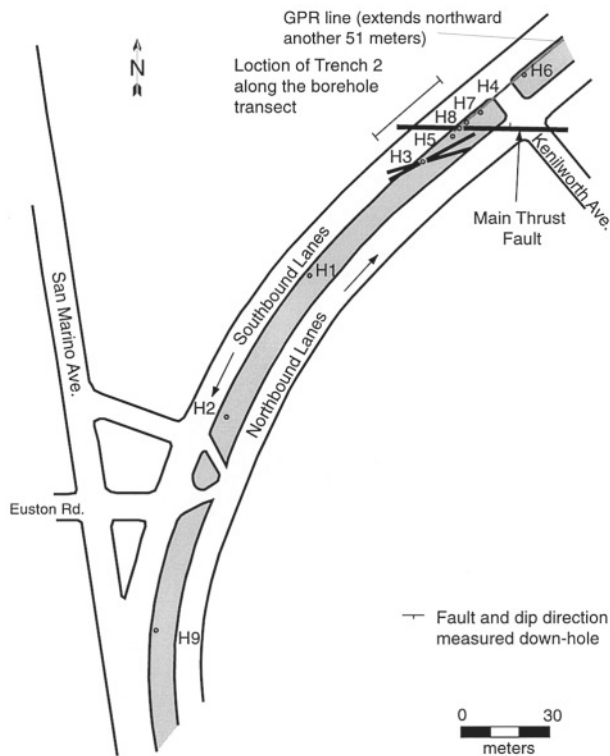


Figure 10. Map of the large-diameter (“bucket auger”) borehole transect at the site of trench T-2. “H” denotes borehole location and number. Faults observed in boreholes H3 and H8 are indicated by thick lines. Dark gray line represents the GPR transect shown in Figure 12.

tween faults b and d are overlain by a sandy pebble to cobble gravel (unit O in Figure 14) of varying thickness (≤ 70 cm). The gravel is overlain by a silty sand (unit P) ~ 30 cm thick and an ~ 8 -cm-thick clayey silt (unit Q), which is in turn covered by a series of silty sands. These units, along with those below it, can be correlated across fault d to the south end of the trench.

At the north end of the trench, the sediments between faults a_2 and b consist of a sequence of sands, granules, and silty fine-grained sands, which overlie a pebbly sand layer, which in turn overlies several gravel deposits. These units gradually dip more steeply southward with depth, and near the base of the trench they are overturned and dip parallel to the 80° -north-dipping fault (Fig. 14).

North of fault a_2 the sediments consist of friable sands and gravels (Fig. 14). Pebble lines within the gravels exposed in the lowest 3 m of the trench indicate that the gravels consist of a series of 10- to 75-cm-thick lenticular channels. Unit R, which overlies these gravel channels, consists predominately of coarse-grained sand to small pebble gravel. The lower part of unit R contains a 25- to 40-cm-thick, discontinuous unit composed of cohesive, silty, very fine-grained sand. Centimeter-scale bedding within this cohesive sand unit is horizontal. The cohesive, fine-grained sandy

unit, and the enclosing coarse-grained sand of unit R, are cut by several vertical, texturally distinct, ~ 70 -cm-long, 1–10-cm-thick lenses of packed coarse-grained sand and granules (collectively labeled unit S in Figure 14). A 30- to 60-cm-thick package of horizontal- to gently south-dipping, fine- to coarse-grained sand, granule, and very small pebble beds (unit T) overlies and truncates the top of all but one of the vertical sand- and granule-filled lenses that cut unit R. The northernmost sand- and granule-filled vertical lens of unit S extends upward across the unit R/unit T contact, all the way to the base of unit U. The upper most few centimeters of this vertical lens consists of unit U material that has apparently fallen into and filled the vertical lens.

The modern A horizon covers the surface of the entire trench. This unit, which maintains a nearly constant, 30- to 40-cm thickness over the entire length of the trench, has a nearly planar base that lies parallel to the present ground surface, and consists of dark brownish-gray to near-black, organic-rich sand with abundant tree and grass roots from modern vegetation.

Age Control. Age control for trench T-2 is provided by nine detrital charcoal samples and two bulk-soil samples (Table 2). With the exception of four samples, all ^{14}C samples recovered from trench T-2 received a standard, acid-base-acid pretreatment designed to remove any organic material that the sample has acquired since burial. Two very small detrital charcoal samples (RFSM 215 and 216; Table 2) and two bulk soil samples (RFGL 3 and 24a; Table 2), however, were deemed to be too delicate for the standard pretreatment, and consequently they received only a single acid wash. Thus, it is possible that these four samples have been contaminated by younger carbon material. However, the two detrital charcoal samples are from a depth of 4.3 m, and the two bulk soil samples are from 2 and 3 m depth. Furthermore, because ~ 1.5 m of material was removed from above the trench during last 100 years (discussed later), the burial depths of these samples suggests that contamination of these samples by young carbon during pedogenesis was probably negligible.

The radiocarbon ages of the bulk soil and detrital charcoal samples (triangles and stars, respectively, in Figure 14; Table 2) indicate that the trench contains a latest Pleistocene geologic record. The bulk soil samples collected from the base and top of the dark bluish-gray to black silt (unit D) yielded ages in radiocarbon years of $>37,300$ yr B.P. and $33,330 \pm 840$ yr B.P., respectively. The two pieces of detrital charcoal that received only the acid pretreatment were collected from a very thin layer of silt at the base of the trench and were combined for analysis because of their small sizes. This combined sample yielded a conventional carbon age of $>27,340 \pm 130$ yr B.P. Two detrital charcoal samples from the charcoal-rich silt overlying unit D yielded ages of $33,660 \pm 530$ and $32,240 \pm 250$ radiocarbon years B.P. (Table 2). Three charcoal samples from unit I, unit O, and a layer of sandy silt located to the south of fault d (stratigraphically above unit O; Figure 16) yielded ages in radio-

Bucket-auger Holes and Location of Trench 2

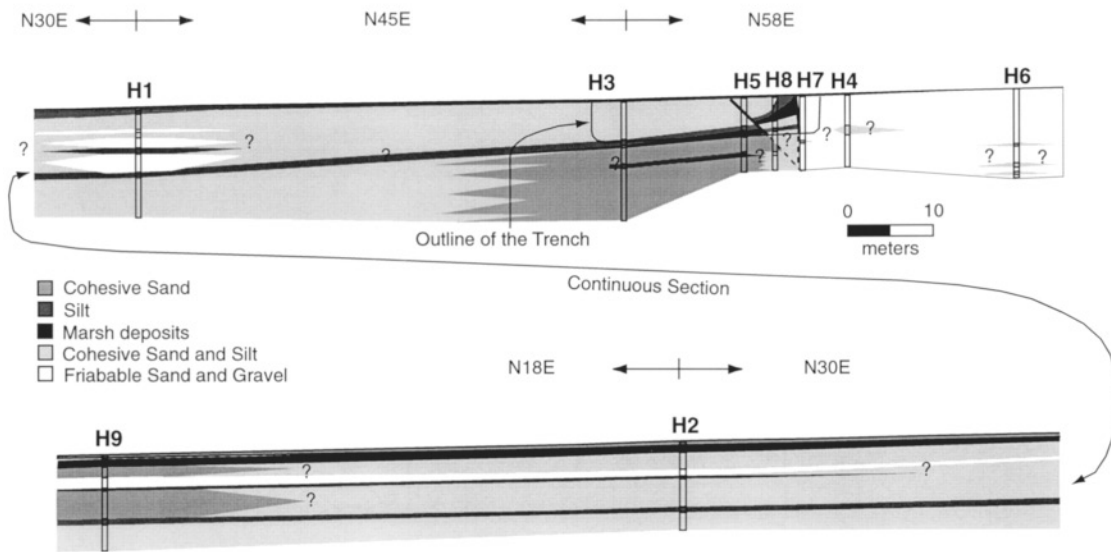


Figure 11. Cross section looking northwest showing a composite log of the nine large-diameter boreholes and the location of the trench T-2. Note that because the borehole transect followed Sierra Madre Boulevard, its orientation changed at three points, as indicated by the black arrows and labels. The ground-penetrating RADAR (GPR) profile discussed in the text was acquired along this line of cross section (see Figure 12).

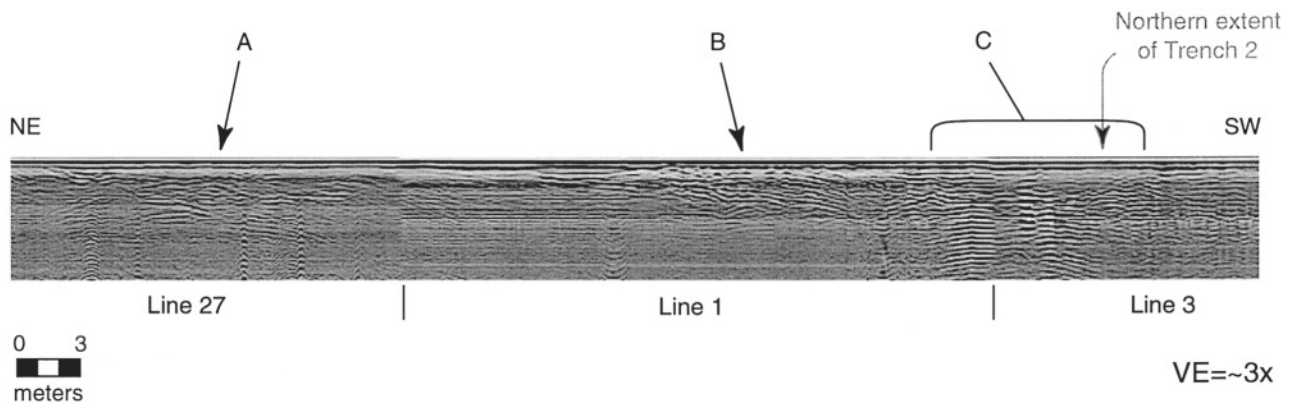


Figure 12. Part of the GPR profile collected at site of trench T-2. Vertical exaggeration is approximately 3:1. Feature A, a gently southwest-dipping feature, is probably a stream channel. Feature B is also gently southwest-dipping, but has a more irregular surface than A. This is probably an artifact of crossing a paved intersection that bisects the median strip of Sierra Madre Boulevard. Feature C denotes a series of vertical changes in reflection intensity and appears to be an ~10-m-wide vertical fault zone. We directly observed the southern two meters of this fault zone in trench T-2 (faults a and b in Figure 13).

carbon years of $32,820 \pm 440$ B.P., $29,900 \pm 160$ B.P., and $27,530 \pm 150$ yr B.P., respectively. Within errors, these seven samples decrease in age up-section, suggesting that they have not been reworked. In the northernmost part of the trench, a detrital charcoal sample from unit T yielded an age of $34,250 \pm 830$ radiocarbon years B.P., and another

sample collected from a gently south-dipping sand bed above unit U yielded $20,350 \pm 90$ yr B.P. These two samples are also in stratigraphic succession, and no reworking is indicated.

All of these ages are older than the maximum calibration age for Calib 3.0.3 (Stuiver and Reimer, 1993). As noted

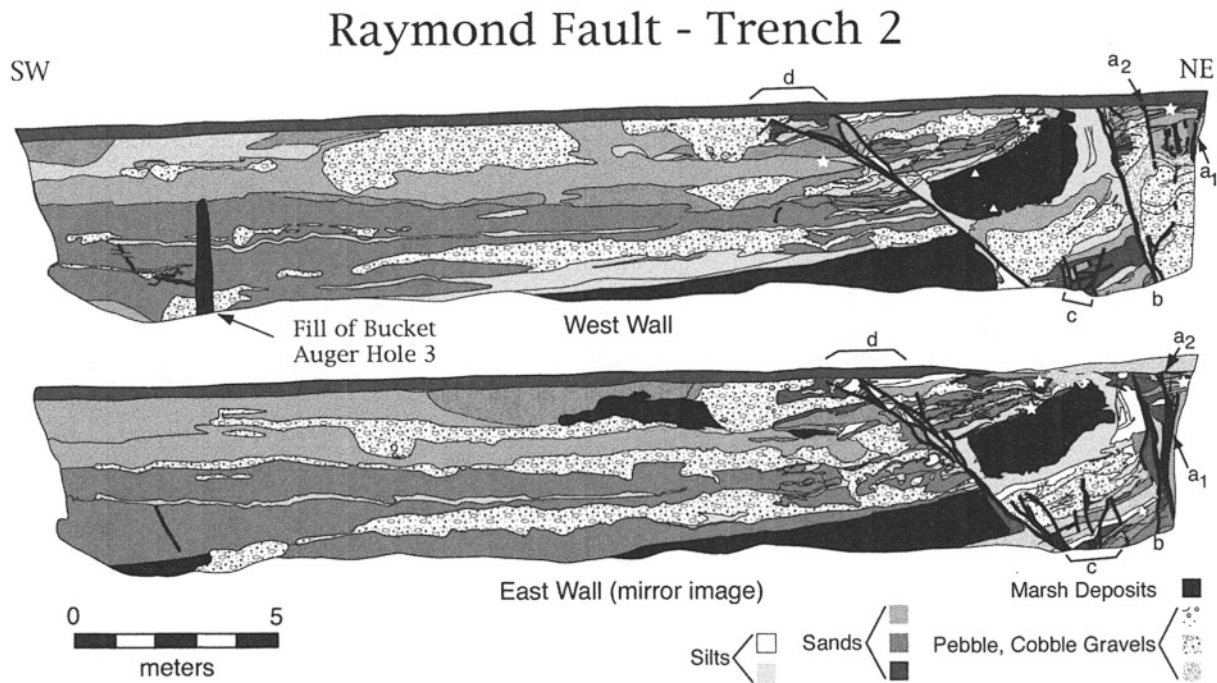


Figure 13. Logs of west and east (mirror image) walls of trench T-2. Heavy black lines labeled a through d indicate the faults discussed in the text. The locations of detrital charcoal and bulk soil samples are indicated by white stars and triangles, respectively (see Figure 14 and Table 2 for ¹⁴C age data).

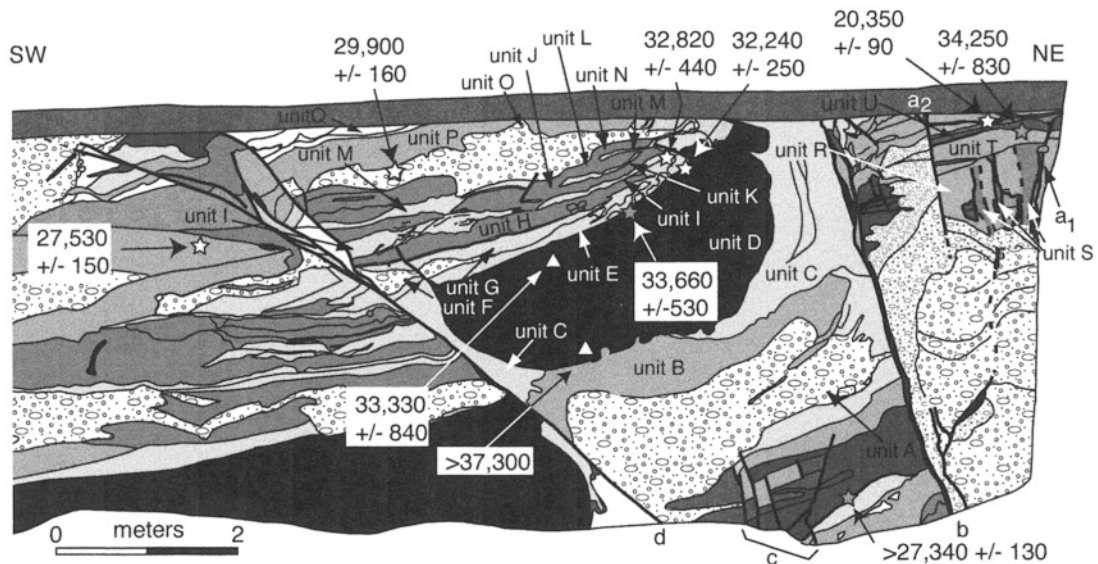


Figure 14. Detail of the north end of the west wall of trench T-2 showing approximate calendric ages of ¹⁴C samples, as estimated from data in Voelker *et al.* (1998) (see text for discussion). Stars and triangles refer to sample locations of detrital charcoal and bulk soil samples, respectively. Samples collected from the east wall have been projected to the west wall for comparison and are represented by gray stars. Capital and lowercase letters designate specific units and faults discussed in the text. Pattern scheme is the same as in Figure 13.

Table 2
C¹⁴ Samples from Trench 2, San Marino, CA

Sample	Location†	Description	Conventional C ¹⁴ Age‡	Approximate Calendric Ages based on Voelker et al. (1998)
RFSM 106 west wall	+ 3.55, + 3.31	Charcoal fragments from charcoal-rich layer above marsh	32,240 ± 250	~38,000
RFSM 108 west wall	+ 3.71, + 3.49	Contorted fine-grained sand; same level as RF SM 102	32,820 ± 440	~39,000
RFSM 110 west wall	+ 8.75, + 2.56	Gray-beige sandy silt south of n-dipping fault	27,530 ± 150	~31,500
RFSM 162 east wall	+ 3.12, + 3.75	Beige silty unit	29,900 ± 160	~34,000
RFSM 185 east wall	+ 3.32, + 2.95	Gray-black charcoal layer on top of marsh	33,660 ± 530	~40,000
RFSM 215 east wall§	+ 0.48, + 0.49	3 cm below top of silt; combined with 216	>27,340 ± 130	~31,000
RFSM 216 east wall§	+ 0.61, + 0.41	From 4 cm below top of gray silt; combined with 215		
RFSM 233 west wall§	+ 0.24–0.34, + 3.79	Could be combined with 234	>20,350 ± 90	~24,000
RFSM 246 east wall	– 0.55, + 3.63	Silty fine-grained sand between fracture bills	34,250 ± 830	~39,000
RF GL3§	9–14	Dark gray sandy silt top of probable marsh deposit	33,330 ± 840	~39,000
RF GL24§	119–124	Medium-dark gray sandy silt; bottom of probable marsh deposit	>37,300	~41,500

*All samples were processed by Beta Analytic, Miami, Florida. All samples were pretreated with acid, alkali and acid washes before analysis, except for those noted by ε. RFSM samples are detrital charcoal or plant material. RF GL samples are bulk soil samples collected from the dark gray-black sandy silt.

†RFSM sample locations given in x,y coordinates of a meter-spaced grid on the original trench logs. RFGL sample locations given in centimeters from the top of the dark gray-black silt deposit. Please see Figures 5 and 9 for exact sample locations on the trench logs.

‡Conventional Dates are reported as radiocarbon years before present (RCYBP), where “present” = 1950 A.D. and include two sigma, or 95% probability, error bars. Samples collected from Trench 2 were too old to calculate calendar ages.

§Indicates sample that was acid-washed only.

earlier, however, we can estimate an approximate calendric age for these samples by applying a correction based on coral and lake sediment age data in conjunction with a geomagnetic model of magnetic flux intensity, together with a comparison of high-resolution sediment records with precisely dated ice cores (Bard *et al.*, 1993; 1998; Laj *et al.*, 1996; Voelker *et al.*, 1998). We compare the AMS ages of all T-2 samples in radiocarbon years B.P. with our estimates of their approximately corrected, calendric ages in Table 2.

These studies indicate that the approximate calendric age of the >37,000 year B.P. samples from the base of unit D is >~41.5 ka. The ~32,240 to 33,700 year B.P. samples from the top of unit D and overlying unit I are associated with a brief period of very high ¹⁴C production rates, with consequent very rapid changes in the rate of change in ¹⁴C production (Voelker *et al.*, 1998). Thus, the approximate calendric ages that we estimate later are probably less reliable than those for older and younger samples. With this caveat in mind, we suggest that the approximate calendric ages of these samples are ~38 to 40 ka. The approximate calendric age of the 29,900 radiocarbon year B.P. sample from unit O is ~34 ka, whereas the approximate corrected age of the 27,530 year B.P. sample from south of fault d is ~31.5 ka. For the 20,350 year B.P. and 34,250 year B.P.

samples from the northernmost part of the trench, we estimate approximate calendric ages of ~24 ka and 39 ka, respectively.

Evidence for Faulting. Four main fault zones were visible in the trench (Figs. 13 and 14). The two northern faults, a and b, both reach the base of the modern A horizon, but only fault b could be traced downward continuously through the gravels in the lower 3 m of the trench. The various strands of fault a are well defined in the upper part of the trench by the sharply defined, vertical, coarse-grained sand- to granule-filled lenses cutting through units R–T at the north end of the trench. However, these vertical lenses, which we interpret as fissure fills, became difficult to trace downward through the friable gravels near the base of the trench. Fault b is near-vertical and juxtapose different lithologic sequences, suggesting that it has experienced significant strike-slip motion.

Fault c, which comprises at least six individual strands in a 1-m-wide zone, is exposed in the lowest meter of the trench. Fault d, in contrast to the predominantly horizontal slip that we infer for the other faults, exhibits ~1.6 m of apparent north-side-up reverse-slip, indicated by restoring the black- to bluish-gray marsh deposits of unit D (black in Figures 13 and 14; assumes no strike-slip). The fault d plane

strikes N86°W and dips 45° N. At ~2 m depth, fault d splays upward into several anastomosing strands that cut up to the base of the modern A horizon.

Interpretation of Trench 2 Results. The base of the A horizon that caps the entire length of the trench is an old railroad grade that was graded during the early 1900s and removed and landscaped in 1951. Assuming that the original ground surface across the trench site was relatively planar, the geometry of the hills on either side of the trench site suggest that ~1.5 to 2 m of material was removed from above the north end of the trench, whereas ≤50 cm appears to have been removed from above the south end of the trench. The latest ¹⁴C Pleistocene ¹⁴C ages recovered from the trench suggest that any Holocene sediments were removed during railroad construction, and therefore there is no record of Holocene earthquakes at this site. The trench does contain, however, an excellent record of at least five latest Pleistocene Raymond fault surface ruptures, as well as at least three shaking-related events that may or may not have been generated by rupture of the Raymond fault itself.

The oldest surface rupture, event 1, is recorded by the upward termination of the six strands of fault c at or below the base of a sand and pebble gravel unit near the base of the trench (unit A in Figure 15). This event tilted some of the sands and gravels cut by the fault strands, but the abrupt thickening, thinning, and disappearance of different sedimentary layers across individual strands suggests that it was predominately a strike-slip event(s). Our crude estimates of the calendric age of the sample from the base of unit D indicate that unit D deposition began before ~41.5

ka (Table 2). Thus, the oldest Raymond fault surface rupture exposed in the trench occurred before ~41.5 ka.

Evidence for events 2, 3, and 4 is found in the sequence of thin sand and silt beds (units E through Q) that overlie unit D. Figure 16 illustrates our semischematic interpretation of the evolution of these strata, beginning with the deposition of a silt unit (unit E) atop the marsh deposits (unit D). Event 2 followed deposition of unit E, and was followed by deposition of a wedge-shaped sandy pebble gravel (unit F) that pinches out between the east and west walls of the trench (Figs. 16(b) and (c)). The wedge shape of unit F indicates that it was deposited against a south-facing slope that we interpret as having been formed by tilting during event 2. Units G and H were subsequently deposited over unit F. The top of silt unit G on the east wall dips more shallowly than its base, indicating that it, in the absence of unit F, was also deposited against a scarp.

Evidence for Event 3 occurs on both walls of the trench, where several faults cut upward through unit H and are truncated by unit I (Figs. 16(c), (d) and (e)). Liquefaction during this earthquake may have caused the convoluted silt stringers within units H and G that were observed on the west wall. The 32,240 ± 250 yr B.P. detrital charcoal age collected from the top of unit D provides a maximum possible age for Event 2, whereas the statistically indistinguishable 32,820 ± 440 yr B.P. age for the detrital charcoal sample from unit I postdates event 3. As noted earlier, our approximate calendric age corrections for these two samples suggest that events 2 and 3 occurred during a brief period of time ~38 to 40 ka.

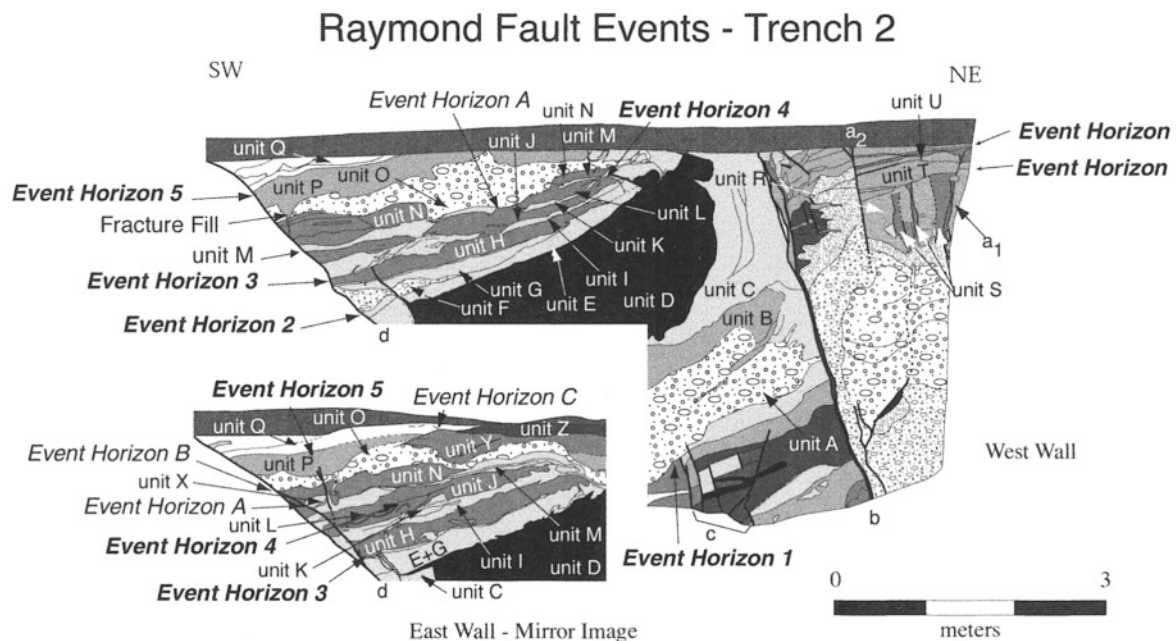


Figure 15. Detail of the north end of the walls of trench T-2 illustrating evidence for the paleoseismic events observed in this trench. Bold numbers refer to Raymond fault events, while shaking-only events are labeled with letters. See Figure 13 for pattern descriptions.

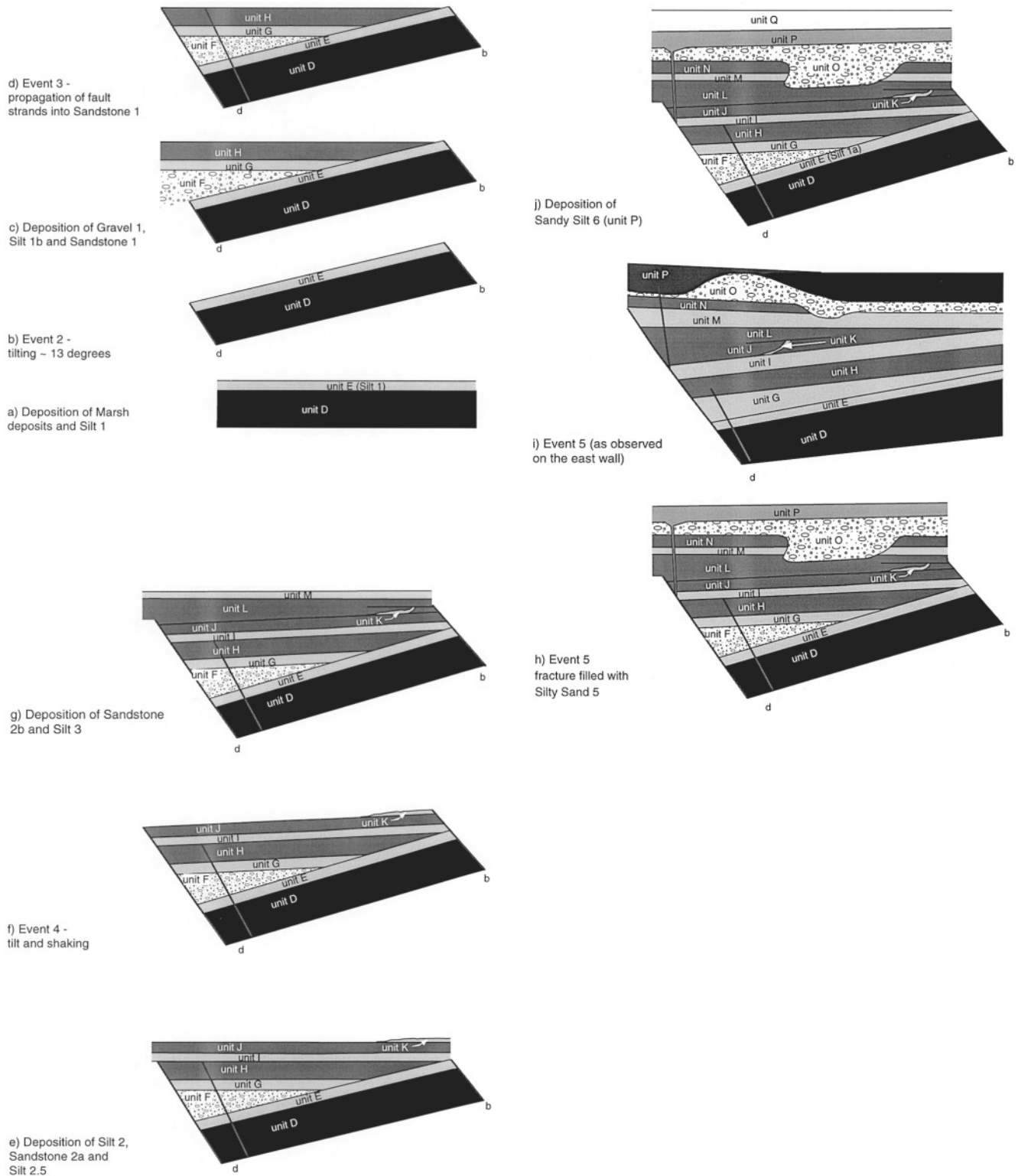


Figure 16. Idealized, sequential sketches of the depositional and seismic events that occurred at trench T-2 following deposition of unit D. Figures (a) through (h) and (j) show the relationships observed on the west wall of the trench, whereas (i) shows Event 5 as it was observed on the east wall of the trench. Figures (i) and (j) represent the same period of time on the west and east trench walls, respectively. Note that Event 4 is manifested as a fracture fill on the west wall, and as several fault splays on the east wall. Event 1 occurred prior to deposition of unit D and is not shown. Patterns are as in Figure 13. Bold, dark gray lines are faults.

Unit I, which postdates event 3, is overlain by the older portion of a sand and a silty unit comprising units J and K (Fig. 16(f)). On both walls of the trench a package of unit K is slumped over unit J. In addition, the sand unit blanketing the unit K slump is a northward-thinning wedge (unit L) that appears to have been deposited against a gently south-facing scarp, unlike the underlying units (Fig. 16(g)). The same earthquake (event 4) that produced the unit K slump probably tilted these units, forming the south-facing scarp. The age of event 4 is bracketed by the $29,900 \pm 160$ radiocarbon years B.P. date from post-event 4 unit O, for which we estimate an approximate calendric age of ~ 34 ka, and the ~ 38 to 40 ka, approximate calendric age for the sample from pre-event 4 unit I. Event 4 was followed by deposition of units L through O.

On the west wall of T-2, event 5 is represented by a fracture filled with silty sand (unit P) that extends upward from the main, north-dipping fault d (Fig. 16(i)). On the east wall, event 5 is expressed by several fault strands that terminate within unit P (Fig. 16(j)). The age of event 5 is constrained by the $29,900 \pm 160$ yr B.P. date from a detrital charcoal sample from unit O just below the event horizon, and by the $27,530 \pm 150$ yr B.P. date from a unit stratigraphically above the event horizon in the footwall of fault d (Figure 14; Table 2). Our estimated calendric ages for these two samples suggest that event 5 occurred between ~ 31.5 and ~ 34 ka (Table 2).

In addition to these five surface ruptures recorded by strata to the south of fault b, the upward terminations of the vertical, sand-, and granule-filled fissures (unit S) at the north end of the trench along strands of fault a record two surface ruptures. One event horizon is located at the base of unit T, as defined by at least three individual unit S faults that terminate at the base of unit T. A younger event horizon occurs within unit U, as defined by a vertical fissure filled with unit U coarse-grained sand and granule material (Fig. 14). The age of the older event is poorly constrained as being older than the $34,250 \pm 830$ yr B.P. unit T sample, for which we estimate a calendric age of ~ 39 ka. The younger event occurred after ~ 39.5 ka, but before deposition of the $20,350 \pm 90$ B.P. sample from above unit U, for which we estimate an approximate calendric age of ~ 24 ka (Fig. 14; Table 2). These crude age constraints do not allow us to distinguish the two events recorded along fault a from the five surface ruptures described already (Fig. 17).

In addition to the five Raymond fault surface ruptures recorded by strata between faults b and d, we observed three slumped packages of strata that we interpret as shaking-induced features that cannot be attributed to the earthquakes described already. We refer to these as events A through C, in order to avoid confusion with surface-rupture designations. These shaking events may or may not have resulted from earthquakes that ruptured the Raymond fault, but nonetheless correspond to strong ground shaking that affected

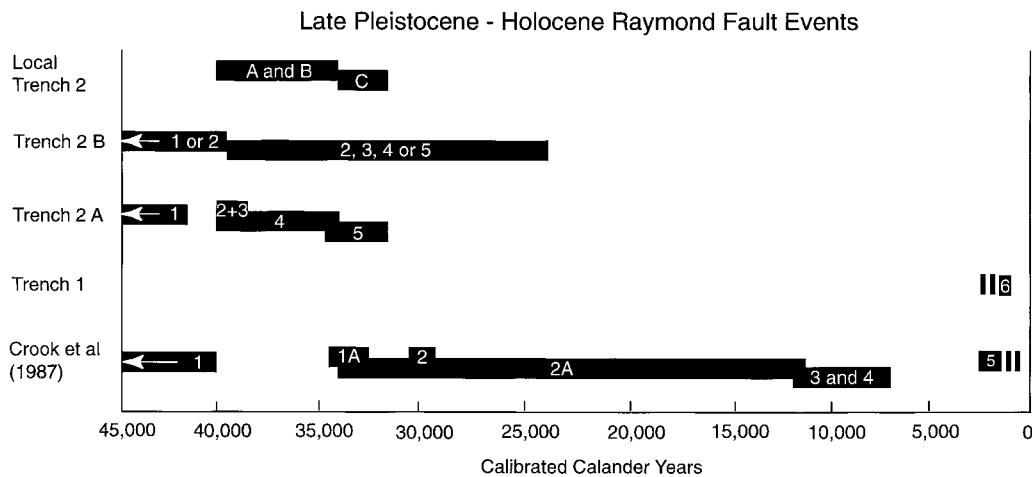


Figure 17. Diagram showing age relationships between the events constrained by this study and by that of Crook *et al.* (1987). Bars represent the maximum calibrated calendar ages. Sample ages up to ~ 18 ka B.P. were calibrated using Calib 3.0 (Stuiver and Reimer, 1993). For older samples, we estimated approximate calendric ages using the ^{14}C production-rate curves in Voelker *et al.* (1998). Arrows indicate undetermined maximum age ranges. "Trench 1" refers to the results of the first trench discussed in our study. "Trench 2A" and "Trench 2B" refer to earthquakes that are interpreted from stratigraphy in the southern and northern portions, respectively, of the Raymond fault zone as observed in trench T-2. "Local Trench 2" refers to events inferred from slumping, liquefaction, and other shaking-induced features observed in this study that cannot be directly attributed to a surface rupture on the Raymond fault. Our approximate calendric age estimates for Raymond fault events discussed by Crook *et al.* (1987) are shown for comparison.

this site. The first shaking event, event A, followed event 4 but occurred before deposition of unit O. This event is identified by slumping of a silt (unit M) on both walls of the trench (Fig. 15). On the west wall the slump surface is a nearly planar rootless “fault” that terminates downward in sandstone 2 and upward at the base of the gravel (unit O). On the east wall the unit M silt occurs as two relatively thick layers (~20-cm-thick) that are connected by a thin (1–2-cm-thick) neck; we suspect that a listric slump surface may have stretched silt M to produce this geometry. These slumps are stratigraphically younger than event 4, and older than the gravel of unit O. Neither slump is associated with tilting of the units below it, and therefore, we interpret these slumps as the result of shaking during an earthquake that did not produce surface rupture on the Raymond fault.

Evidence for event B is seen on the east wall of the trench in the form of a nearly vertical, ribbon-shaped silt slump (unit X, Fig. 15). This silt cuts across the sand and silt of units M and N, and is overlain by gravel (unit O). Because the slump cuts unit M and N, the shaking event must be younger than event A. Likewise, because it is overlain by the gravel (unit O), this event is older than event 5. As with event A, event B does not appear to have been accompanied by tilting, so it may have also been a non-Raymond fault shaking event. Because shaking events A and B occurred after deposition of unit I and before deposition of unit O, our estimated calendric age corrections for the charcoal samples obtained from units I and O (discussed earlier) indicate that shaking events A and B occurred between ~34 ka and ~38 to 40 ka (Table 2).

Shaking event C is recorded on the by apparent thrust fault displacement of several sand and gravel layers (units O, P, and Q) over two other gravel layers (units Y and Z, Fig. 15). Event C, which was not observed on the west wall, did not produce perceptible tilting on the east wall, and therefore was probably also the result of shaking during a local non-Raymond fault earthquake. This event can be constrained as occurring between $27,530 \pm 1.50$ and $29,900 \pm 160$ radiocarbon years B.P. (Table 2). Our calendric age estimates for these samples bracket the age of shaking event C between ~31.5 ka and ~34 ka (Table 2).

Discussion

The well-defined fault zone geomorphology of the Raymond fault supports the earlier interpretation of Jones *et al.* (1990) that the Raymond fault is a predominately left-lateral strike-slip fault, in contrast to earlier suggestions by Buwalda (1940) and Crook *et al.* (1987) that it accommodates predominately reverse motion with a component of strike slip. Specifically, the consistent left deflection of numerous drainages by as much as 400 m and the focal mechanism for the 1988 earthquake confirm major left-lateral strike-slip on the Raymond fault. Moreover, we suggest that the east-northeast-trending ridge of crystalline rock at the east end of the fault appears to have been transported westward, out-

ward from the San Gabriel Mountain front, along the Raymond fault. This geometry suggests that the apparent offset of the basement ridge approximates the maximum total strike-slip on the Raymond fault.

Our geomorphologic zone III differs from zones to the east and west in that it does not exhibit a consistently well-developed south-facing scarp. We interpret this as an indication that zone III has experienced more purely strike-slip motion than the transpressional sections of the fault to the west. The westward-increasing height of the south-facing scarp west of zone III is a result of motion through the Raymond Hill–Huntington Estate restraining bend, at which the fault undergoes a 25° change in strike (Fig. 2).

Although our geomorphologic studies have failed to reveal a discernible direct connection between the Raymond and the Hollywood faults, the similar orientation and kinematics of the two faults (both accommodate predominately left-lateral strike-slip motion with subordinate reverse slip) suggests that a connection may exist. Weber *et al.* (1980) described north-facing scarps approximately along strike of the Hollywood fault on the eastern edge of the Los Angeles River floodplain. Although these scarps may be fluvial in origin (Dolan *et al.*, 1997), they are superposed on an overall south-facing slope in the alluvial-fluvial deposits that is directly along strike with, and to the east of, the well-established location of the Hollywood fault to the west of the Los Angeles River floodplain. This east-trending, south-facing slope also overlies a major, very sharp gravity gradient that extends from the western part of the Raymond fault system, westward beneath the Los Angeles River, and along the Hollywood fault to the west (Fig. 2; Chapman and Chase, 1979). These observations suggest that there may be a through-going fault connection between the Raymond and Hollywood faults, approximately where it has been mapped by Weber *et al.* (1980) and Dibblee (1989). If such a connection exists, then the Raymond fault, together with the Hollywood and Santa Monica faults to the west, form part of a continuous, >80-km-long system of oblique-reverse left-lateral faults that extends across the northern edge of Los Angeles basin (Fig. 1; Dolan *et al.*, 1995, 1997, 2000a, 2000b).

Previous authors (Weber *et al.*, 1980; Crook *et al.*, 1987; Dibblee, 1989) have suggested that the Eagle Rock fault connects with the Raymond fault somewhere near Raymond Hill, but these interpretations are based on very sparse and equivocal geomorphologic indicators, as well as the presence of several bedrock faults. The absence of clear-cut geomorphologic indications for a direct Eagle Rock–Raymond fault connection suggests the possibility that the Eagle Rock fault may be much less active than the Raymond fault. If this is the case, then the Raymond fault may not act as a tear-fault, transferring reverse slip from the Sierra Madre fault to the Verdugo fault, as has been previously suggested (e.g., Dolan *et al.*, 1995). This, however, remains an open question, and the connection between the Eagle Rock and Verdugo fault awaits further study. In contrast, the connec-

tion between the Raymond fault and the Sierra Madre fault is a structurally complex, but well-expressed, zone at the east end of the offset crystalline basement ridge (Fig. 2; Crook *et al.*, 1987).

Our paleoseismologic data from trench T-1 indicate that the most recent surface rupture on one strand of the fault occurred before ~A.D. 1050, and sometime after B.C. 8050. These broad age constraints on the most recent event can be narrowed by using our minimum age for this event together with published data from an earlier study of the fault by Crook *et al.* (1987). Their trenches near Sunny Slope reservoir, 2.5 km west of trench T-1 (Fig. 2), revealed a series of sharply defined, ~50-cm-long (top to bottom), 10- to 20-cm-wide fissures filled with black, peaty marsh deposits. These near-vertical fissure fills extend down to ~2 m depth, and project downward into several well-defined, steeply north-dipping faults. These features were interpreted by Crook *et al.* (1987) as direct evidence of the most recent surface rupture on the Raymond fault. The organic-rich fill from one of these fissures yielded a calibrated, bulk-sample calendric age of B.C. 189 +212/-261 (their sample C-6; our calibration using Calib 3.03; Stuiver and Reimer, 1993; Table 1). This date provides a maximum age for the most recent Raymond fault surface rupture. Given that the peaty deposits fell into the fissures, they must have been accumulating for some period of time before the earthquake. This suggests that the age of the sample from the fissure fill is older than the age of the most recent event, by some unknown amount of time. In summary, the most recent Raymond fault surface rupture occurred sometime after deposition of the B.C. 189 +212/-261 sample from the Crook *et al.* (1987) trench, but before deposition of the ~A.D. 1050 sample from the unfaulted deposits in the southern part of trench T-1.

Our trench T-2 revealed a latest Pleistocene paleoseismologic record of at least five surface ruptures on the Raymond fault, as well as three shaking events that may be related to ruptures other area faults. Although we did not recover a Holocene record at this trench site, we can use the ages of the latest Pleistocene events to comment on the recurrence characteristics of the Raymond fault. The published ages of the five to eight Raymond fault surface ruptures interpreted by Crook *et al.* (1987) are based primarily on bulk-soil radiocarbon ages from three of their trenches. As with the pre-~18,000 yr B.P. radiocarbon samples from our two trenches, we can use the estimates of ^{14}C production rates reported in Voelker *et al.* (1998) to estimate the approximate calendric ages for the five to eight surface ruptures reported by Crook *et al.* (1987) (all event ages from Crook *et al.* (1987) are denoted below by the prefix CR; e.g., CR-1 is Event 1 of Crook *et al.*, 1987).

In Figure 17 we compare our approximate calendric age corrections for the Crook *et al.* (1987) event ages with the approximate calendric age estimates for our Events 1 through 5. These results show that the five to eight Crook *et al.* (1987) events occurred between ~40 ka and ~2 ka,

yielding a maximum average recurrence interval for this period of ~5,700 to ~10,000 years. Our estimates of approximate calendric ages for the Crook *et al.* (1987) events indicate that between three and five of their events (CR-2A[?], CR-3, CR-4, Cr-4A[?], and CR-5) have occurred since the ~31.5 ka minimum possible age for our Event 5. Thus, over this interval the measured average occurrence interval based on the Crook *et al.* (1987) data is ~7,400 and 15,000 years. Crook *et al.* (1987) recognized the possibility, however, that some events may have remained undetected in their study, and speculated that the actual average recurrence interval was much shorter than their measured interval. They suggested 3000 years as a plausible recurrence interval for large events on the Raymond fault.

Our data show that for the ~10,000-year-long period between ~41.5 and ~31.5 ka, the measured average recurrence interval on the Raymond fault for our Events 2–5 was ≤ 3300 years (Fig. 17). The minimum interval is unconstrained over this time interval, and may be much shorter than 3300 years. Comparison of our maximum measured recurrence interval with the Crook *et al.* (1987) results described already implies either that (1) the ~41.5 to ~31.5 ka events were part of a temporally anomalous “cluster,” and thus that the recurrence interval on the Raymond fault is highly irregular; or alternatively, (2) if the recurrence interval is approximately constant at ≤ 3300 years, then more than half of all Raymond fault surface ruptures since ~31.5 ka have not yet been detected.

The 20 km length of the fault, coupled with an 80° fault dip and a seismogenic thickness of ~16 km (Jones *et al.*, 1990), yields a total fault plane area of ~325 km². Regressions of moment-magnitude versus fault-plane area and average slip (Wells and Coppersmith, 1994; Dolan *et al.*, 1995) indicate that rupture of the Raymond fault in its entirety could produce a $M_W \sim 6.7$ event with ~50 to 100 cm of average slip. No reliable geological estimates of the slip rate on the Raymond fault are available at this time. Walls *et al.* (1998), however, using best-fit models of GPS geodetic results from the northern Los Angeles metropolitan region, have suggested a slip rate of 1.5 ± 0.5 mm/yr on the Raymond fault. Combining this slip-rate estimate with the expected 50 to 100 cm of average slip suggests that if all strain on the Raymond fault was released during $M_W 6.7$ events, then such events would recur every ~250 to 1000 years. This estimate is much shorter than the measured average recurrence intervals discussed earlier, suggesting either that (1) the slip rate estimate of Walls *et al.* (1998) is too high; or (2) most ($\geq 80\%$ to 90%) of the earthquakes that have occurred on the Raymond fault during the past ~40,000 years have not yet been recognized; or (3) the Raymond fault ruptures together with adjacent faults (e.g., the Hollywood-Santa Monica, Sierra Madre, and Verdugo-Eagle Rock faults) in larger, but less frequent events than would be expected for rupture of the Raymond fault by itself.

Paleoseismologic data from the central Sierra Madre and Verdugo faults are as yet too poorly constrained to com-

pare with Raymond fault events, but the $\sim 7\text{--}9.5$ ka age of the most-recent surface rupture on the Hollywood fault (Dolan *et al.*, 2000a) conflicts with the $\sim 1\text{--}2$ ka age for the most recent Raymond fault surface event. These observations suggest that the Raymond fault did not rupture together with the Hollywood fault during its most recent surface rupture. These data do not, of course, preclude the possibility that earlier ruptures did involve both of these faults.

Conclusions

The geomorphically well-expressed Raymond fault extends for 20 km in a gentle convex-to-the-south arc through the San Gabriel Valley northeast of Los Angeles. Geomorphologic data, including left-lateral stream deflections, shutter ridges, sag ponds, pressure ridges, and an apparent 3.4-km-long left-lateral offset of a basement ridge, coupled with the focal mechanism and steeply north-dipping (80°) aftershock zone of the 1988 Pasadena earthquake, all indicate that the Raymond fault is a left-lateral strike-slip fault (Buwald, 1940; Weber *et al.*, 1980; Crook *et al.*, 1987; Jones *et al.*, 1990; this study). Common, consistently south-facing scarps along much of the fault are primarily the result of motion through a major restraining bend along the central part of the fault in southwestern Pasadena, as well as a possible subordinate compressional component of motion, particularly along the western part of the fault.

Whereas the confluence of the Raymond fault with the Sierra Madre fault at its eastern end is well defined structurally and geomorphically, the interactions between the Raymond fault and the Hollywood and Eagle Rock faults are less well defined. On the basis of published mapping (Weber *et al.*, 1980; Dibblee, 1989), gravity data (Chapman and Chase, 1979), and our geomorphologic analysis we believe there may be a complicated, but through-going fault trace between the Raymond fault and the Hollywood fault, along strike to the west. If this is true, the Raymond-Hollywood-Santa Monica fault zone would constitute a $>80\text{-km}$ -long, thorough-going system of oblique reverse left-lateral faults (Fig. 1; Dolan *et al.*, 1995).

Our paleoseismologic trench data indicate that the most recent surface rupture along one strand of the Raymond fault occurred before \sim A.D. 1050. Coupled with published results from an earlier study of the fault, these data indicate that the most recent surface rupture on the Raymond fault occurred between ~ 1000 and 2000 years ago. Another of our trenches revealed evidence for at least five latest Pleistocene surface ruptures, including four events closely spaced in time between 31.5 and 41.5 ka. The $\leq 3300\text{-year}$ -long, maximum average recurrence interval for these five events is much shorter than the ~ 5700 to $\sim 10,000$ year latest Pleistocene-Holocene measured average recurrence interval for the fault based on our reanalysis of paleoseismologic data in Crook *et al.* (1987). It is similar, however, to the $\sim 3000\text{-year}$ recurrence interval suggested by Crook *et al.* (1987) on the basis of their assumption that an unknown number of events

had remained undetected in their study. A comparison of our paleoseismologic data with published results indicates that either (1) the 31.5–41.5 ka events were part of a temporally anomalous “cluster,” and that the recurrence interval for the fault is irregular; or (2) the recurrence interval for the Raymond fault is relatively constant at ≤ 3300 years, in which case more than half of all Raymond fault events that have occurred during the past $\sim 40,000$ years have not yet been detected.

One of the major outstanding questions facing seismic hazard planners in Los Angeles is whether or not faults such as the Raymond can rupture simultaneously with adjacent faults, producing very large earthquakes similar to the 1992 M_w 7.3 Landers multifault rupture (Sieh *et al.*, 1993). The Raymond fault interacts directly with three major faults, the Sierra Madre fault to the northeast, the Eagle Rock–Verdugo fault to the northwest and the Hollywood fault to the west. An earlier investigation indicates that the Hollywood fault produced its most recent surface rupture between ~ 7000 and ~ 9500 years ago (Dolan *et al.*, 2000a), in conflict with the age of $\sim 1,000\text{--}2,000$ years of the most recent Raymond fault surface rupture. These observations suggest that the Raymond fault did not rupture together with the Hollywood fault during the most recent event. The existing data, however, do not preclude earlier simultaneous rupture of these two faults.

Acknowledgments

The authors wish to acknowledge Debbie Bell, John Penido, and the staff of the City of San Marino, as well as John Provine and the Los Angeles County Arboretum staff for paving the way for us to excavate on their respective properties. Ann Blythe, Karl Mueller, David Bowman, and Jamie Gardner provided helpful editorial comments. Special thanks to Richard Crook, Robert Hill, and Richard Proctor for providing us with data from their earlier investigations of the Raymond fault, and to Jerry Treiman at the California Division of Mines and Geology and Steven Lipshie at the Los Angeles County Public Works and for allowing us access to their departments' aerial photo and map collections. Thanks also to Brian Wernicke for his help with the permitting. This field investigation could not have been completed without the help of the following people: Joe Barr, Jeff Beard, David Bowman, Steve Colbert, Arie Jan Doets, Bob DeGroot, Margaret Glasscoe, Ross Hartleb, Soparkh Khalsa, Ilene Cooper, Wayne Marko, Wende Owen, Matthew Ragan, Brooks Ramsdell, Meredith Robertson, Allan Tucker, and Joel Wedberg. Donn Schwarzkopf of Terra Geosciences conducted the GPR study. This research was supported by the Southern California Earthquake Center (SCEC). SCEC is supported by NSF Cooperative Agreement EAR-8920136 and USGS Cooperative Agreements 14-08-0001-A0899 and 1434-HQ-97AG01718. SCEC publication number 506.

References

- Argus, D. F., M. B. Heflin, A. Donnellan, F. H. Webb, D. Dong, K. J. Hurst, D. C. Jefferson, G. A. Lyzenga, M. M. Watkins, and J. F. Zumberge (1999). Shortening and thickening of metropolitan Los Angeles measured and inferred using geodesy, *Geology* **27**, 703–706.
- Bard, E., M. Arnold, R. G. Fairbanks, and B. Hamelin (1993). ^{230}Th – ^{234}U and ^{14}C ages obtained by mass spectrometry on corals, *Radiocarbon* **35**(1), 191–199.

- Bard, E., M. Arnold, B. Hamelin, N. Tisherat-Laborde, and G. Cabroch (1998). Radiocarbon calibration by means of mass spectrometric $^{230}\text{Th}/^{234}\text{U}$ and ^{14}C ages of corals. An updated base including samples from Barbados, Mururoa and Tahiti, *Radiocarbon* **40**, 1085–1092.
- Buwalda, J. P. (1940). Geology of the Raymond Basin: report to the City of Pasadena Water Dept., 9 plates, 131p.
- Chapman, R. H., and G. W. Chase (1979). Geophysical investigations of the Santa Monica-Raymond fault zone, Los Angeles County, California, *Calif. Div. Mines Geol. Open-File Rep. 79-16*, E-1–E-30.
- Crook, R., Jr., C. R. Allen, B. Kamb, C. M. Payne, and R. J. Proctor (1987). Quaternary geology and seismic hazard of the Sierra Madre and associated faults, western San Gabriel Mountains, in *Recent Reverse Faulting in the Transverse Ranges, California, U.S. Geol. Surv. Prof. Pap. 1339*, 27–63.
- Dibblee, T. W. (1989a). Geologic Map of the Pasadena Quadrangle, Los Angeles County, California, Dibblee Geological Foundation.
- Dibblee, T. W. (1989b). Geologic Map of the Los Angeles Quadrangle, Los Angeles County, California, Dibblee Geological Foundation.
- Dolan, J. F., and K. Sieh (1992). Tectonic geomorphology of the northern Los Angeles basin: seismic hazards and kinematics of young fault movement, in *Engineering Geology Field Trips: Orange County, Santa Monica Mountains, and Malibu, Guidebook and Volume*, P. L. Ehlig and E. A. Steiner (Editors), Assoc. Eng. Geol., pp. B-20–B-26.
- Dolan, J. F., K. Sieh, T. K. Rockwell, R. S. Yeats, J. Shaw, J. Suppe, G. Huftile, and E. Gath (1995). Prospects for larger or more frequent earthquakes in greater metropolitan Los Angeles, California, *Science* **267**, 199–205.
- Dolan, J. F., K. Sieh, T. K. Rockwell, P. Gupta, and G. Miller (1997). Active tectonics, paleoseismology and seismic hazards of the Hollywood fault, northern Los Angeles Basin, California, *Bull. Geol. Soc. Am.* **109**, 1595–1616.
- Dolan, J. F., D. Stevens, and T. K. Rockwell (2000a). Paleoseismologic evidence for an early- to mid-Holocene age of the most recent surface rupture on the Hollywood fault, Los Angeles, California, *Bull. Seism. Soc. Am.* **90**, 334–344.
- Dolan, J. F., K. Sieh, and T. K. Rockwell (2000b). Late Quaternary activity and seismic potential of the Santa Monica fault system, Los Angeles, California, *Geol. Soc. Am. Bull.* **112**, 1559–1581.
- Hill, R. L., E. C. Spottle, R. H. Chapman, G. W. Chase, J. H. Bennett, C. R. Real, R. C. Slade, G. Borchardt, and F. H. Weber (1979). Earthquake hazards associated with faults in the greater Los Angeles Metropolitan Area, Los Angeles County, California, including faults in the Santa Monica-Raymond, Verdugo-Eagle Rock and Benedict Canyon fault zones, *California Division of Mines and Geology Open File Report 79-16 LA*.
- Jones, L. M., K. E. Sieh, E. Hauksson, and L. K. Hutton (1990). The 3 December 1988 Pasadena earthquake: evidence for strike-slip motion on the Raymond Fault, *Bull. Seism. Soc. Am.* **80**, 474–482.
- Laj, C., A. Mazaud, and J.-C. Duplessy (1996). Geomagnetic intensity and ^{14}C abundance in the atmosphere and ocean during the past 50 kyr, *Geophys. Res. Lett.* **23**, 2045–2048.
- Scientists of USGS/SEEC (1994). The magnitude 6.7 Northridge, California, earthquake of 17 January 1994, *Science* **266**, 389–397.
- Sieh, K., L. Jones, E. Hauksson, K. Hudnut, D. Eberhart-Phillips, T. Heaton, S. Hough, K. Hutton, H. Kanamori, A. Lilje, S. Lindvall, S. F. McGill, J. Mori, C. Rubin, J. A. Spotila, J. Stock, H. K. Thio, J. Treiman, B. Wernicke, and J. Zachariasen (1993). Near-field investigations of the Landers Earthquake Sequence, April to July 1992, *Science* **260**, 171–176.
- Shaw, J. H., and P. Shearer (1999). An elusive blind-thrust fault beneath metropolitan Los Angeles, *Science* **283**, 1516–1518.
- Shaw, J. H., and P. M. Suppe (1998). A Blind-Thrust Fault beneath metropolitan Los Angeles identified from seismic reflection profiles and precise earthquake locations, Presented at American Geophysical Union Annual Meeting, November 1998, San Francisco, California.
- Stuiver, M., and P. J. Reimer (1993). Radiocarbon Calibration Program Revision 4.1.2, *Radiocarbon* **35**, 215–230.
- Vedder, J. G., H. G. Greene, S. H. Clarke, and M. P. Kennedy (1986). Geologic map of mid-southern California continental margin (map 2A), California continental margin geologic map series (area 2 of 7; map sheet 1 of 4), H. Greene and M. Kennedy (Editors), U.S. Geological Survey, Menlo Park, California, and California Division of Mines and Geology, Sacramento, California, 1:250,000.
- Voelker, A. H., M. Sarthein, P. M. Grootes, H. Erlenkeuser, C. Laj, A. Mazaud, M.-J. Nadeau, M. Schleicher (1998). Correlation of marine ^{14}C ages from the nordic seas with the GISP2 isotope record: implications for ^{14}C calibration beyond 25 ka BP, *Radiocarbon* **40**, 517–534.
- Walls, C., T. Rockwell, K. Mueller, Y. Bock, S. Williams, J. Pfanner, J. Dolan, and P. Fang (1998). Escape tectonics in the Los Angeles metropolitan region and implications for seismic risk, *Nature* **394**, 356–360.
- Weber, F. H., J. H. Bennett, R. H. Chapman, G. W. Chase, and R. B. Saul (1980). Earthquake hazards associated with the Verdugo-Eagle Rock and Benedict Canyon fault zones, Los Angeles County, California, *Calif. Div. Mines Geol. Open-File Rep. 80-10 LA*.
- Wells, D., and K. Coppersmith (1994). New empirical relationships among magnitude, rupture length, rupture width, rupture area, and surface displacement, *Bull. Seism. Soc. Am.* **84**, 974–1002.
- Wright, T. L. (1991). Structural geology and tectonic evolution of the Los Angeles Basin, in *Active-Margin Basins*, Biddle, K. T. (Editor), AAPG Memoir 52, 35–106.
- Ziony, J. I., and L. M. Jones (1989). Map showing late Quaternary faults and 1978–84 seismicity of the Los Angeles region, U.S. Geol. Surv. Misc. Field Studies Map MF-1964, scale 1:250,000.

Department of Earth Sciences
University of Southern California
Los Angeles, CA 90089-0740
(J. D.)

Manuscript received 15 June 1999.